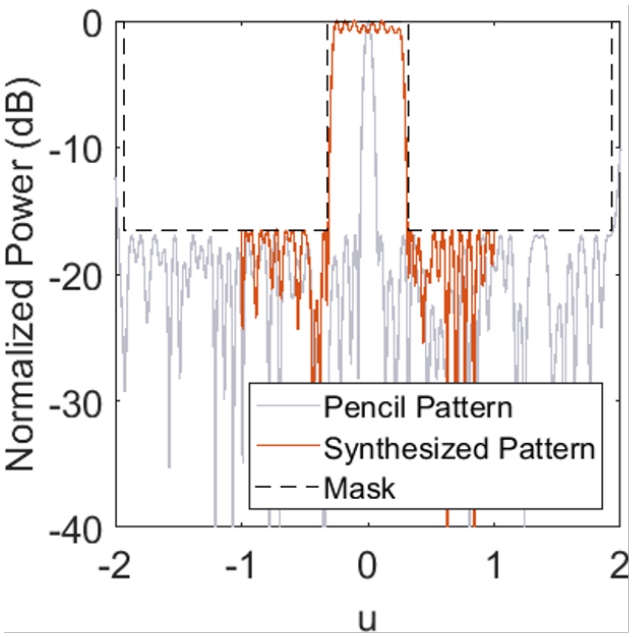

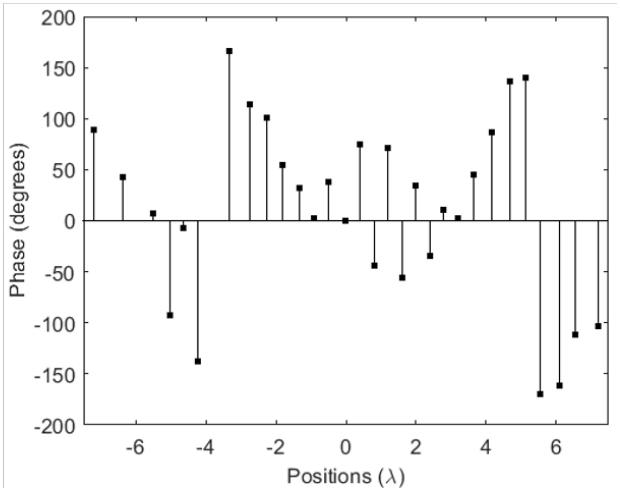

Synthesis of Isophoric Sparse Antenna Arrays

A Method Evaluation for Reconfigurable Transmit Beams

Master's thesis in Electrical Engineering

ERIK ANGERT SVENSSON & EBBA OLSSON

DEPARTMENT OF ELECTRICAL ENGINEERING
CHALMERS UNIVERSITY OF TECHNOLOGY
Gothenburg, Sweden 2021
www.chalmers.se

Master's thesis 2021

Synthesis of Isophoric Sparse Antenna Arrays

A Method Evaluation for Reconfigurable Transmit Beams

ERIK ANGERT SVENSSON
EBBA OLSSON

CHALMERS
UNIVERSITY OF TECHNOLOGY

Department of Electrical Engineering
Division of Communications, Antennas, and Optical Networks
Antenna Systems
Chalmers University of Technology
Gothenburg, Sweden 2021

Synthesis of Isophoric Sparse Antenna Arrays
A Method Evaluation for Reconfigurable Transmit Beams
ERIK ANGERT SVENSSON
EBBA OLSSON

© Erik Angert Svensson and Ebba Olsson, 2021.

Supervisors:
Milena Anguelova, Saab AB
Bengt Svensson, Saab AB
Axel Flinth, Electrical Engineering, Chalmers

Examiner:
Rob Maaskant, Electrical Engineering, Chalmers

Master's thesis 2021
Department of Electrical Engineering
Division of Communications, Antennas, and Optical Networks
Antenna Systems
Chalmers University of Technology
SE-412 96 Gothenburg
Telephone +46 31 772 1000

Cover: Results from the synthesis of a reconfigurable sparse antenna array, able to transmit both a pencil beam and a flat-top beam.

Typeset in LaTeX
Gothenburg, Sweden 2021

Synthesis of Isophoric Sparse Antenna Arrays
A Method Evaluation for Reconfigurable Transmit Beams
ERIK ANGERT SVENSSON
EBBA OLSSON
Department of Electrical Engineering
Chalmers University of Technology

Abstract

Synthesis of antenna arrays radiating both narrow and shaped beams using uniform amplitude excitations are of high interest for transmit applications. Reducing the number of antenna elements by introducing a sparsity can reduce cost, weight and complexity of a system. To this end, several different methods have been suggested in the literature. An area of special interest is the introduction of a minimum distance between elements required in practical implementations.

In this thesis, two methods for optimizing isophoric sparse antenna arrays under a minimum distance constraint are evaluated; an iterative convex optimization method and a method based on a density taper approach. The methods are used for optimization of positions and phases of antenna elements with the objective of producing pencil beams, cosecant squared beams, flat-top beams as well as reconfigurable beams. Both methods gave satisfactory results for the pencil beam synthesis. For the two shaped beam forms, the density taper technique turned out to give lower sidelobes than the convex optimization method, possibly due to the difficulty in reformulating a non-convex problem into a convex one. A conclusion drawn from the results is that the problem is large and has many local minima, thereby requiring a careful setup and problem definition.

Keywords: sparse antenna arrays, aperiodic, isophoric, uniform-amplitude, convex optimization, density taper, pencil beam pattern, cosecant squared beam pattern, flat-top beam pattern, reconfigurable beam pattern

Acknowledgements

First of all, we would like to express our great gratitude to our two supervisors at Saab, Bengt Svensson and Milena Anguelova, as well as our academic supervisor at Chalmers, Axel Flinth. The weekly discussions with all of you have been tremendously valuable, interesting and of great support. This master's thesis would have been beyond the bounds of possibility without the engagement from all of you.

Moreover, we would like to thank Saab Surveillance in general, for the opportunity to perform this intriguing master's thesis, and our two Saab managers Mats Högberg and Ulrika Svahn in particular. Your interest in the work progress has been highly encouraging.

Finally, we would like to send our special thanks to our families and friends, not only for the support during this project, but also for all our years at Chalmers. Nothing of this would have been possible without you.

Erik Angert Svensson & Ebba Olsson, Gothenburg, June 2021

Contents

List of Figures **xi**

List of Tables **xiii**

1 Introduction **1**
1.1 Summary of Previous Studies . . . 1
1.2 Purpose and Scope . . . 2
1.3 Ethical Considerations . . . 3
1.4 Thesis Outline . . . 3

2 Theory **5**
2.1 Antenna Arrays . . . 5
2.1.1 Array Factor . . . 6
2.1.2 Power Pattern . . . 8
2.1.3 Power Pattern Factorization . . . 8
2.1.4 Power Pattern Beam Shapes . . . 9
2.1.5 Filled Linear Arrays with $\lambda/2$ Spacing . . . 10
2.1.6 Sparse Arrays . . . 10
2.1.7 Directivity . . . 11
2.1.8 Amplitude and Phase Tapers . . . 12
2.2 Optimization . . . 12

3 Methods **15**
3.1 Expansion on Previous Studies . . . 15
3.2 General Problem Setup . . . 16
3.3 Convex Optimization Method . . . 17
3.3.1 Pencil Beam Synthesis . . . 17
3.3.2 Shaped Beam Synthesis with Phase Tapering . . . 20
3.4 Deterministic Method . . . 21
3.4.1 Density Taper . . . 22
3.4.2 Arbitrary Reference Source . . . 23

4 Implementation and Assessment of Results **25**
4.1 Case 1: Pencil Beam with Minimum SLL . . . 26
4.1.1 Convex Optimization Method . . . 26
4.1.2 Deterministic Method . . . 27
4.2 Case 2: Pencil Beam with Maximum Sparsity . . . 28

4.2.1 Convex Optimization Method 28
4.2.2 Deterministic Method 29
4.3 Case 3: Shaped Beam Cosecant Squared Pattern 31
4.3.1 Convex Optimization Method 31
4.3.2 Deterministic Method 32
4.4 Case 4: Shaped Beam Flat-top Pattern 33
4.4.1 Convex Optimization Method 34
4.4.2 Deterministic Method 34
4.5 Case 5: Reconfigurable beam 36
4.5.1 Convex Optimization Method 36
4.5.2 Deterministic Method 37
4.6 Pencil Beam Steering 39
4.7 General Discussion 40
4.8 Recommended Future Extensions 41

5 Conclusion **43**

References **45**

A Element Positions and Phases **I**
A.1 Case 1: Pencil Beam with Minimum SLL I
A.2 Case 2: Pencil Beam with Maximum Sparsity III
A.3 Case 3: Shaped Beam Cosecant Squared Pattern VI
A.4 Case 4: Shaped Beam Flat-top Pattern XI
A.5 Case 5: Reconfigurable Beam XVII

List of Figures

2.1 Antenna array setup 6
2.2 Phase array steering 7
2.3 Selection of zeros 9
2.4 Taylor distribution 12

3.1 SLL decreasing with number of elements 19

4.1 Case 1, convex method 26
4.2 Case 1, deterministic method 27
4.3 Case 2, convex method, SLL $= -13\,\mathrm{dB}$ 28
4.4 Case 2, convex method, SLL $= -17\,\mathrm{dB}$ 29
4.5 Case 2, deterministic method, SLL $= -13\,\mathrm{dB}$ 30
4.6 Case 2, deterministic method, $-17\,\mathrm{dB}$ 30
4.7 Case 3, convex method 32
4.8 Case 3, deterministic method 33
4.9 Case 4, convex method 34
4.10 Case 4, deterministic method 35
4.11 Case 5, convex method, flat-top beam 37
4.12 Case 5, deterministic method, cosecant squared reconfigurable beam . 38
4.13 Case 5, deterministic method, flat-top reconfigurable beam 39
4.14 Pencil beam steering 40

A.1 Case 1, element positions I
A.2 Case 2, element positions, SLL $= -13\,\mathrm{dB}$ III
A.3 Case 2, element positions, SLL $= -17\,\mathrm{dB}$ IV
A.4 Case 3, convex method, $N = 40$ VI
A.5 Case 3, deterministic method, $N = 40$ VIII
A.6 Case 3, deterministic method, $N = 30$ X
A.7 Case 4, convex method, flat-top, $N = 40$ XI
A.8 Case 4, convex method, flat-top, $N = 34$ XIII
A.9 Case 4, deterministic method, $N = 40$ XIV
A.10 Case 4, deterministic method, $N = 30$ XVI
A.11 Case 5, convex method, flat-top, $N = 40$ XVII
A.12 Case 5, convex method, flat-top, pencil beam, $N = 40$ XVII
A.13 Case 5, convex method, flat-top, $N = 34$ XIX
A.14 Case 5, convex method, flat-top, pencil beam $N = 34$ XIX
A.15 Case 5, deterministic method, cosecant squared, $N = 40$ XXI

A.16 Case 5, deterministic method, cosecant squared, pencil beam, $N = 40$ XXI
A.17 Case 5, deterministic method, cosecant squared, $N = 30$ XXIII
A.18 Case 5, deterministic method, cosecant squared, pencil beam, $N = 30$ XXIII
A.19 Case 5, deterministic method, flat-top, $N = 40$ XXV
A.20 Case 5, deterministic method, flat-top, pencil beam, $N = 40$ XXV
A.21 Case 5, deterministic method, flat-top, $N = 30$ XXVII
A.22 Case 5, deterministic method, flat-top, pencil beam, $N = 30$ XXVII

List of Tables

A.1 Case 1, convex method II
A.2 Case 1, deterministic method III
A.3 Case 2, convex method, SLL $= -13\,\mathrm{dB}$ IV
A.4 Case 2, convex method, SLL $= -17\,\mathrm{dB}$ V
A.5 Case 2, deterministic method, SLL $= -13\,\mathrm{dB}$. V
A.6 Case 2, deterministic method, SLL $= -17\,\mathrm{dB}$. VI
A.7 Case 3, convex method, $N = 40$ VII
A.8 Case 3, deterministic method, $N = 40$ IX
A.9 Case 3, deterministic method, $N = 30$ X
A.10 Case 4, convex method, $N = 40$ XII
A.11 Case 4, convex method, $N = 34$ XIII
A.12 Case 4, deterministic method, $N = 40$ XV
A.13 Case 4, deterministic method, $N = 30$ XVI
A.14 Case 5, convex method, flat-top, $N = 40$ XVIII
A.15 Case 5, convex method, flat-top, $N = 34$ XX
A.16 Case 5, deterministic method, cosecant squared, $N = 40$ XXII
A.17 Case 5, deterministic method, cosecant squared, $N = 30$ XXIV
A.18 Case 5, deterministic method, flat-top, $N = 40$ XXVI
A.19 Case 5, deterministic method, flat-top, $N = 30$ XXVIII

1

Introduction

Antenna arrays consist of multiple antenna elements, each of which may have an individual amplitude and phase excitation. Together, the antenna elements can be used to transmit both narrow beams and radiation patterns of arbitrary shape, as well as to steer the beam in a desired direction. The synthesis and design of antenna arrays has historically been a relevant topic, and it remains so today. The versatility of controlling the radiation pattern electrically is of high interest for a variety of antenna applications including telecommunications, satellite communications and radar applications [1], [2, p. 1].

A typical, conventional, filled array consists of elements positioned at a distance of half a wavelength apart. An array with the same number of elements, but with varying inter-element distances, is referred to as aperiodic. Furthermore, a sparse array refers to an array containing fewer elements than its filled equivalent. Introducing sparsity among the antenna elements enables the reduction of cost, weight and complexity of the antenna array, while closely replicating the beamwidth and maximum sidelobe level of a conventional filled array [3].

In the available literature, there is a variety of different methods for synthesizing both aperiodic antenna arrays with minimum sidelobes and sparse antenna arrays. However, many applications require a uniform amplitude excitation of the antenna elements in order to operate efficiently during transmission [1]. Arrays with equal amplitude excitation are referred to as isophoric. For practical implementations, another requirement is a minimum inter-element distance. Research including these two constraints is less commonly found in the literature compared to methods neither restricting excitation amplitudes nor element positions.

1.1 Summary of Previous Studies

In [3–5], synthesis of isophoric sparse arrays via an iterative norm minimization technique based on Compressive Sensing is described. Using the L_1 and L_∞ norms to regularize the solution, a convex minimization problem is set up to optimize the array excitations. The L_1 norm induces sparsity in the solution, while the L_∞ norm induces a uniform amplitude. By a certain balancing between these two norms the

excitations should hence end up with uniform amplitudes and sparse locations.

A second convex optimization approach is presented in [6], where an iterative algorithm solving a convex optimization problem is used. Because of the convex problem, a linearization of the problem is required. The method deals solely with uniform amplitude and equiphased arrays for pencil beams. On the whole, there are many ways to implement a method using convex optimization.

Another approach is presented and expanded upon in a series of articles by the authors of [7]. Here, a deterministic approach based on a classical density taper technique is used to obtain starting values for an optimization problem. In addition, a mathematical trick is used to calculate a large number of equivalent starting positions. All the described methods optimize the solution to fulfill a desired power pattern.

While the literature provide rigorous methods which produce results within their scope, they collectively leave an important practical consideration unanswered. In order to successfully manufacture antenna arrays, a minimum distance is required between the antenna elements. The distance is needed to account for both the physical size of each antenna element, as well as to reduce the mutual coupling between them [8, p. 285]. The focus of this report is therefore a sparse isophoric antenna array having a minimum inter-element distance as a requirement.

A more detailed description and evaluation of the methods is found in Chapter 3.

1.2 Purpose and Scope

With the available literature as a starting point, the purpose of the project is to examine different methods for synthesizing radiation patterns for sparse isophoric arrays, as well as for filled isophoric arrays with different beam shapes. In particular, two different methods will be examined; one using iterative convex optimization and one with a deterministic approach. In order to evaluate and compare the outcome of the two methods, the goal has been to study the synthesis of certain beam patterns and the reconfiguration between two different patterns with a common antenna. Of particular interest is how the methods respond to the introduction of a minimum inter-element distance constraint, while simultaneously enforcing uniform amplitude.

The solutions are required to have a minimum distance of 0.4 times the wavelength of the radiation between adjacent elements. This is necessary in order to effectively realize the results in practice and avoid large mutual coupling effects. Furthermore, all antenna elements are excited with uniform amplitude to allow for maximum power transmission.

There are several key limitations to the examinations carried out in this thesis. First of all, the antenna is synthesized in only one dimension. This simplification has areas of implementation of its own and is not hindering in terms of showing

that the problem is conceptually solvable in two or three dimensions. Secondly, no mutual coupling effects are considered in the implementations of the methods. The reason for this is that it would considerably complicate the calculation of the beam pattern and therefore make the optimization problem very large. Enforcing the relatively large inter-element distance of 0.4 times the wavelength reduces the effects of mutual coupling, making the solutions a good starting point for further optimization.

1.3 Ethical Considerations

There are several possible ethical, societal and ecological aspects to be taken into consideration regarding this project. The aim of the development work is to reduce the number of elements used in a design to achieve a given performance. This would lead to a decreased material usage and a lower cost of production. Because of the lower cost and material usage, products utilizing the concepts of this project have the possibility of becoming more widely used for different purposes, possibly differing from common applications of today. The methods presented in this report are of a very general nature, and their use have the possibility of improving many antenna systems.

Considering the ethical aspects of the project, it is important to understand that the research is carried out in association with the defence company Saab AB, meaning that further developments from the results may be used in products with military purposes.

The project work itself is performed in its entirety using simulations in software, thereby reducing material waste. The results however, are dependent on prototype testing to verify the applicability of the results.

1.4 Thesis Outline

The outline of the thesis is structured according to the following. In Chapter 2, general theory needed for the project is introduced. The chapter is divided into a first part about antenna array theory and a second part about optimization problems in general. Some theory about performance measures is also given here. In Chapter 3, a more detailed description of the two methods used is given. Previous studies are also described in greater detail. In Chapter 4, the results from the implementations of the methods are presented together with a discussion and evaluation. Finally, in Chapter 5, a summarizing conclusion is given, whereafter the Appendix contains all antenna element positions and phases corresponding to the presented results, both in the form of tables and figures.

2

Theory

In the following chapter, the theory that has been used throughout the project is presented. First, some background is given on antenna arrays and thereafter the theory behind the two different optimization methods studied is introduced.

2.1 Antenna Arrays

Multiple antenna elements acting together are referred to as an antenna array [9, p. 333]. The elements are placed stationary relative each other and may be individually excited with a current of varying amplitude and phase. There are four possible parameters affecting the radiation pattern of an array [8, p. 285]:

1. Element positions
2. The excitation amplitude of individual elements
3. The excitation phase of individual elements
4. The radiation pattern of individual elements

The far-field function $\mathbf{F}(\hat{\mathbf{r}})$ produced by the antenna array can be expressed as the superposition of the radiation patterns from each individual antenna element according to [9, p. 335-336]

$$\mathbf{F}(\hat{\mathbf{r}}) = \sum_{n=1}^{N} A_n e^{j\Phi_n} \mathbf{G}_n(\hat{\mathbf{r}}) e^{jk\mathbf{r}_n \cdot \hat{\mathbf{r}}}, \tag{2.1}$$

where j is the imaginary unit, $\mathbf{G}_n(\hat{\mathbf{r}})$ is the element far-field function, which is the radiation pattern of an isolated antenna element. Furthermore, A_n and Φ_n correspond to the excitation amplitude and phase respectively, $\mathbf{r}_n$ is the observation point of element n with direction $\hat{\mathbf{r}}$, N is the number of elements in the array and $k = 2\pi/\lambda$ is the wavenumber where λ is the wavelength.

In this project, only one-dimensional antenna arrays are studied. Such an array is presented in Figure 2.1. Equation (2.1) can be applied to one-dimensional setups, which will be modelled using the array factor presented next.

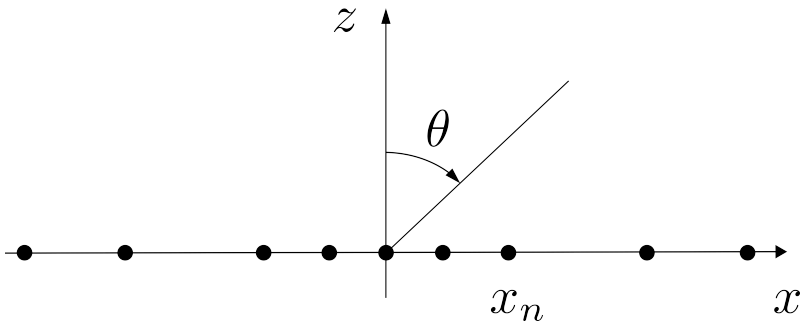

Figure 2.1: One-dimensional antenna array. The dots represent antenna elements placed at position x_n along the x-axis and the far-field angle θ measured from the z-axis.

2.1.1 Array Factor

Making the assumption that all element patterns are equal, the element factor can be placed outside the summation in Eq. (2.1). This leaves only the so called array factor AF, which for the one-dimensional array in Figure 2.1 can be described as

$$AF(\theta) = \sum_{n=1}^{N} w_n e^{jk\sin(\theta)x_n} \tag{2.2}$$

with the weights $w_n = A_n e^{-j\Phi_n}$. The variables θ and x_n are the far-field angle and element position respectively, according to Figure 2.1. When evaluating the far-field pattern for the different methods, the array factor alone is of interest. The element factor $\mathbf{G}_n(\hat{\mathbf{r}})$ only contributes with a constant scaling if it is independent of n [8, p. 288].

The main beam can be moved in space, which is referred to as steering. For an antenna array this can be done without any mechanical motion [10, ch. 20.1]. The steering of the antenna pattern is accomplished by exciting the antenna elements with a progressive phase shift

$$\Delta\Phi_n = k\sin(\theta_s)x_n, \tag{2.3}$$

where θ_s is the steering angle [10, ch. 20.2]. See Figure 2.2 for an illustration.

The far-field is commonly expressed as a function of $u = \sin(\theta)$, rather than as a function of the angle itself. This transformation is valid only in the so called visible region $u \in [-1, 1]$. The coordinate transformation ensures that the array factor only sees a translation in the u-coordinate when the lobe is steered. When the possibility of steering is required, the model must be valid both in the visible region and the invisible region outside of $u \in [-1, 1]$. In order to allow modelling of both a maximum steering angle $\theta_s = 90°$, together with a maximum observation angle $\theta = -90°$ of the array factor, the u-coordinates of interest are in fact $u \in [-2, 2]$. Note that the steering and observation angles are opposite each other.

The boundaries of the region $u \in [-2, 2]$ can be motivated by the following example.

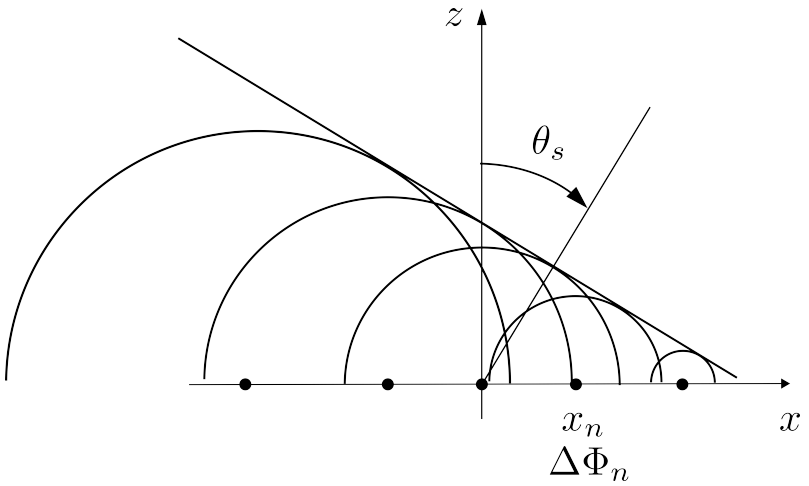

Figure 2.2: Steering of antenna array pattern by element phase shift $\Delta\Phi_n$. The phase front is tangential to the equi-phase positions of the individual radiating electric fields.

Considering Eq. (2.2), steering the array to $\theta_s = 90°$ requires a phase shift of

$$\Delta\Phi_n = k\sin(90°)x_n = kx_n \tag{2.4}$$

such that $w_n = e^{-j\Delta\Phi_n} = e^{-jkx_n}$ in the most simple case [2, p. 16]. Inserting this in Eq. (2.2) for the observation angle $\theta = -90°$ results in

$$AF(-90°) = \sum_{n=1}^{N} e^{-jkx_n}e^{-jkx_n} = \sum_{n=1}^{N} e^{-jk2x_n}. \tag{2.5}$$

Identification with the u-coordinate in e^{jkux_n}, u is seen to be equal to -2. From this, the conclusion can be drawn that in order to ensure the validity of the antenna pattern over the complete visible region for steering angles up to $\pm 90°$, the array factor needs to be calculated for $u \in [-2, 2]$ as

$$AF(u) = \sum_{n=1}^{N} w_n e^{jkux_n}. \tag{2.6}$$

An interesting note can be made regarding the array factor. A continuous distribution of weights can be sampled in points using the Dirac delta function δ according to

$$\sum_{n=1}^{N} w_n \delta(x - x_n). \tag{2.7}$$

The Fourier transform of the Dirac delta function in the above equation is

$$\mathcal{F}\left(\delta(x - x_n)\right)(u) = e^{-jux_n}. \tag{2.8}$$

Using the linearity of the Fourier transform, the Fourier transform of the distribution of weights can be expressed as

$$\mathcal{F}\left(\sum_{n=1}^{N} w_n \delta(x - x_n)\right) = \sum_{n=1}^{N} w_n e^{-jux_n}. \tag{2.9}$$

This Fourier transform has similarities to the array factor. By introducing a rescaling of u in Eq. (2.8) to $-ku$, the Fourier transform of the distribution of weights is equal to the array factor in Eq. (2.6). Consequently, the array factor can be interpreted as the Fourier transform of the distribution of weights.

2.1.2 Power Pattern

The array factor presented in the previous section is a complex property describing the shape of the transmitted beam. However, what is physically transmitted is a power, which is often represented in a power pattern on a logarithmic scale [8, p. 25]. The normalized power pattern is given by the power density along a constant radius and can be calculated from the array factor according to

$$P(u) = |AF(u)|^2. \tag{2.10}$$

This power definition gives rise to an interesting property described in the next section.

2.1.3 Power Pattern Factorization

A unique power pattern can be described by a multitude of array factors having different excitations. Knowledge about the different array factors provides a possibility to choose the most suitable alternative for a given problem. The array factors can be determined by first factorizing the power pattern in Eq. (2.10) according to

$$P(u) = AF(u)AF^*(u) \tag{2.11}$$

where $(\cdot)^*$ represents the complex conjugation [11, p. 111]. The factorization is not unique, which as stated above means that various array factors can produce the same power pattern. In fact, for an equi-spaced array, it is possible to find all array factors corresponding to a specific power profile using an algebraic trick. By writing Eq. (2.6) as

$$AF(u) = \sum_{n=0}^{N-1} w_n e^{jkudn} \tag{2.12}$$

and making the variable substitution $z = e^{jkud}$, the polynomial

$$AF(z) = \sum_{n=0}^{N-1} w_n z^n \tag{2.13}$$

can be formed. Now, the roots z_0 of this polynomial are related to the roots $z_{0,\text{flipped}}$ of the AF^* polynomial as

$$z_{0,\text{flipped}} = \frac{1}{z_0^*}. \tag{2.14}$$

The relationship in Eq. (2.14) is shown to hold algebraically by first expanding $(AF(z))^*$ according to

$$(AF(z))^* = \left(\sum_{n=0}^{N-1} w_n z^n\right)^* = \sum_{n=0}^{N-1} (w_n z^n)^* = \sum_{n=0}^{N-1} w_n^* z^{-n}, \tag{2.15}$$

and then letting $AF(z_0) = 0$. Inserting the roots $z_{0,\text{flipped}}$ into AF^*, Eq. (2.15) can be rewritten as

$$AF^*(z_{0,\text{flipped}}) = AF^*\left(\frac{1}{z_0^*}\right) = \sum_{n=0}^{N-1} w_n^*(z_0^*)^n = \sum_{n=0}^{N-1} (w_n z_0^n)^*$$
$$= \left(\sum_{n=0}^{N-1} w_n z_0^n\right)^* = (AF(z_0))^* = 0.$$

Hence, the roots flipped according to Eq. (2.14) are also roots to $AF(z)AF^*(z)$ and therefore to P. By choosing one in each pair of roots $(z_0, z_{0,\text{flipped}})$ as shown in Figure 2.3, 2^M unique polynomials can be created. Here, M is the number of original roots not lying on the unit circle [12]. Each polynomial correspond to a distinct array factor.

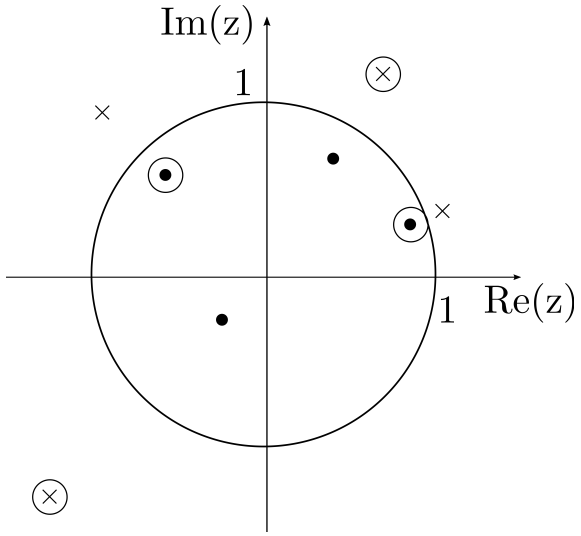

Figure 2.3: From each pair of roots flipped around the unit circle, one is selected, resulting in 2^M different combinations. z_0 is represented by dots and $z_{0,\text{flipped}}$ is represented by crosses. The circled root is selected.

The final goal of the optimizations performed in this project is for the transmit beams, that is the power patterns, to take certain predetermined shapes. The three considered beam shapes are presented henceforth.

2.1.4 Power Pattern Beam Shapes

The most common shape of the power pattern is the so called pencil beam pattern [9, p. 4]. It has a characteristic narrow main lobe beam combined with low sidelobes. Antennas transmitting pencil beams are also called spot-beams antennas. This is because of the small spot such antennas illuminate on the surface of the earth, when located on satellites.

A flat-top beam pattern is a power pattern with a wider main lobe than the pencil beam. Apart from the width, which may be several times larger than that of the

pencil beam, the main lobe also has a flat top. More formally the main lobe top has ideally a constant power. The flatness of the top can be characterized by the so called ripple, which is the power difference between the maximum and minimum power in the main lobe top region. The less ripple, the flatter the beam top.

The cosecant squared radiation pattern is given by [13, p. 9]

$$G(\theta) = \left(\frac{\csc \theta}{\csc \theta_1} \right)^2, \tag{2.16}$$

where θ_1 is the half power beam width (HPBW) where the cosecant squared pattern begins. This is the width of the main lobe where it has reached half-power compared to the main lobe maximum value which corresponds to $-3\,\mathrm{dB}$ [8, p. 26]. The cosecant squared beam pattern is useful in for example air-surveillance radar applications due to the reflected power being independent of the target position in either height or distance [9, p. 4].

The antenna array optimization for synthesizing the presented shapes is done by changing the positions x_n and the phases Φ_n of each element in order to achieve a suitable array factor and related power pattern. Before introducing the optimization, one of the most important special cases of antenna arrays is studied, namely filled linear arrays. Also, the concept of sparse arrays is presented.

2.1.5 Filled Linear Arrays with $\lambda/2$ Spacing

The standard user case of an array is to place the elements with a uniform distance of $\lambda/2$ in between. A reason for this spacing is that the array factor given in Eq. (2.6) is periodical in $u = \lambda/d$, where d is the spacing between the elements.

The lobes that appear due to this periodicity are called grating lobes [8, p. 297]. Since the coordinates of interest are $u \in [-2, 2]$ due to steering, the periodicity of the array factor larger than $u = 2$ is desired. This is achieved for $d = \lambda/2$ in the case of an infinite array. The first sidelobe level for a filled array with uniform amplitude and phase excitation is at $-13.2\,\mathrm{dB}$ compared to the main lobe maximum, and the HPBW in degrees is given by

$$HPBW \approx \frac{50.6\lambda}{L} \tag{2.17}$$

where L is the size of the array and $L \gg \lambda$ [8, p. 415].

2.1.6 Sparse Arrays

A sparse array is an array having an average element spacing larger than $\lambda/2$, and hence fewer elements for a given array aperture size compared to the conventional filled array presented in the previous section. The main lobe beamwidth is mainly related to the maximum dimensions of the array, and therefore it is possible to maintain a similar beamwidth compared to the reference case of a filled array [2,

p. 92]. The drawback is a reduction in gain roughly proportional to the fraction of elements removed, since the gain is directly related to the aperture area [2, p. 92]. The varying element-to-element distance gives rise to pseudo grating lobes which will generally appear spread out between the u-values $1/d_{\max}$ and $1/d_{\min}$, where $d_{\max}$ and $d_{\min}$ denote the maximum and minimum inter-element distances respectively. The desire to reduce the number of elements and hence construct sparse arrays are what motivates the investigation done in this report. To find the optimal element positions and phases of sparse arrays to reduce pseudo grating lobes is not a trivial problem, but the key to achieving useful power patterns.

2.1.7 Directivity

In order to give a fair representation of the resulting power patterns, directivity is a good measure of performance. Directivity quantifies the ability of an antenna to concentrate radiation in a certain direction and will be used later on to evaluate the results of the synthesized pencil beams [8, p. 40]. More specifically, it is the ratio between the radiation intensity in a given direction (most often the direction with maximum intensity) $U_{\max}(\theta)$, and the average radiation intensity over all directions, $U_{\text{avg}}(\theta)$. The radiation intensity for a linear antenna array is given by [8, p. 38]

$$U(\theta) = \left[(AF)_n\right]^2, \tag{2.18}$$

where $(AF)_n$ is the normalized array factor. Furthermore, $U_{\text{avg}}(\theta)$ is equal to the total power radiated by the antenna array, P_{rad}, divided by the area of a sphere in steradians, $A = 4\pi$, which can be computed from the following [8, p. 38]:

$$\begin{aligned} U_{\text{avg}}(\theta) &= \frac{P_{\text{rad}}}{4\pi} = \frac{1}{4\pi}\int_{-\pi}^{\pi}\int_{-\pi/2}^{\pi/2} U(\theta)\cos\theta d\theta d\phi \\ &= \frac{1}{4\pi}\int_{-\pi}^{\pi}\int_{-\pi/2}^{\pi/2} \left[(AF)_n\right]^2\cos\theta d\theta d\phi \\ &= \frac{1}{2}\int_{-\pi/2}^{\pi/2} \left[(AF)_n\right]^2\cos\theta d\theta \end{aligned} \tag{2.19}$$

To be consistent, the variable substitution $u = \sin\theta$ is made. This yields $du = \cos\theta d\theta$ and the integral in (2.19) may be evaluated in terms of u according to:

$$U_{\text{avg}}(u) = \frac{1}{2}\int_{-1}^{1} U(u)du = \frac{1}{2}\int_{-1}^{1}\left[(AF)_n\right]^2 du. \tag{2.20}$$

The directivity is therefore given in decibels by

$$D = 10\log_{10}\left(\frac{U_{\max}}{U_{\text{avg}}}\right). \tag{2.21}$$

The last aspect of antenna arrays presented before introducing the relevant optimization theory are so called amplitude and phase tapers. In the next section, their relevance to the elements and power pattern is explained.

2.1.8 Amplitude and Phase Tapers

In order to achieve a satisfactory sidelobe level (SLL), beam shape and steering angle, different amplitude and phase tapers can be used. The tapers can be interpreted as current distributions on continuous line-sources. A continuous line-source can be approximated by a discrete-element array such that a smaller average element spacing yields a better approximation of the continuous source [8, p. 387]. This way, amplitude and phase tapers dictate the excitation of each individual antenna element. In this project, the amplitude was required to be uniform for all elements, however, the amplitude taper presented in this section can be used as a tool during optimization.

A particular taper of interest for the pencil beam cases in this work is the Taylor distribution, see Figure 2.4. A Taylor distribution is an amplitude taper, developed from a Dolph-Chebyshev distribution, which provides a smooth tradeoff between main- and sidelobe levels for optimal narrow beam width patterns [14]. The inner sidelobes obtained by this distribution are maintained at a constant level, while the outer sidelobes decrease monotonically [8, p. 408]. The Taylor distribution is available in MATLAB through the function *taylorwin* defined by three parameters: the number of sampling points, the SLL parameter SLL_{Taylor} and the number of sidelobes maintained at a constant level $\bar{n}$.

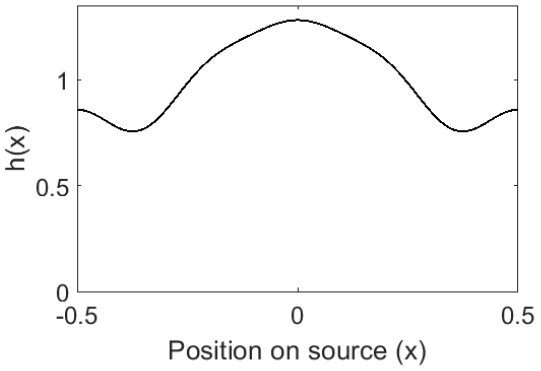

Figure 2.4: Taylor distribution plotted with MATLAB function *taylorwin* for 1000 points, $SLL_{\text{Taylor}} = -20\,\text{dB}$ and $\bar{n} = 5$.

Phase tapers are commonly used to determine the steering angle of the array as showed in Eq. (2.4) [2, p. 1].

2.2 Optimization

The problem of finding the most suitable antenna element positions and phases with respect to a variety of conditions may be formulated as an optimization problem. The problem constraints determines what can be demanded of the final solution. Constraints that can be considered include for example a minimum gain of the main lobe, a maximum width of the main lobe, an upper bound of the sidelobes or a completely predetermined antenna array power pattern from which the synthesized pattern may not differ by more than a certain value defined by the ripple. If the problem is formulated in an accurate way with feasible constraints, it may be solved with known methods.

The mathematical formulation of a general optimization problem is given by [15, p. 1]

$$\begin{array}{ll} \text{minimize} & f_0(\boldsymbol{x}) \\ \text{subject to} & f_i(\boldsymbol{x}) \leq b_i, \quad i = 1, ..., m \end{array} . \tag{2.22}$$

Here $f_0 : \mathbb{R}^n \to \mathbb{R}$ is the objective function, with the optimization variable vector $\boldsymbol{x}$ as argument. The constraint functions $f_i : \mathbb{R}^n \to \mathbb{R}$ are bounded by or equal to the constants b_i. The optimal solution of the problem (2.22) is the vector $\boldsymbol{x}_{\text{opt}}$ which yields the smallest value of the objective function while still satisfying the constraints.

A convex optimization problem is a subclass of optimization problems where both the objective and constraint functions are convex [15, p. 7]. A function $g(x)$ is convex if a line between any two points on its graph lies *above* the graph itself. In mathematical terms this definition is equivalent with the function fulfilling the inequality

$$g(\alpha x + \beta y) \leq \alpha g(x) + \beta g(y), \tag{2.23}$$

for all $x, y \in \mathbb{R}^n$ and all $\alpha, \beta \in \mathbb{R}$ with $\alpha + \beta = 1$ and $\alpha, \beta \geq 0$. A very important property of convex optimization problems is that they only have one global solution [15, p. 138]. This property makes it less dependent on for example initial values in the problem compared to non-convex optimization methods which may produce non-optimal solutions due to many local minima.

Further, due to the existence of robust and efficient solvers for convex optimization problems, it might be advantageous to turn an optimization problem into a convex problem. This would enable an efficient solution procedure. One such solver is the MATLAB package CVX which may be used for solving the mentioned convex optimization problems [16].

However, the convex optimization method also have some undesirable properties. For example, all optimization problems are not convex in their original versions. To use convex optimization, such problems must be approximated as a convex problem and will no longer correspond to the original formulation.

In this report some special limitations of the convex optimization are relevant. To begin with, the problem involves the array factor which contains a sum of complex exponential functions, see Eq. (2.6). What is to be optimized is the power pattern in Eq. (2.10), with the optimization variables being the element positions and their applied phases. Such an objective function is not convex but could be, if, for example, it was linearized with respect to the optimization variables. A linearization of the objective function can be done with the help of a Taylor expansion, and the details on this are presented in Section 3.3.

Another limitation with the method concerns the constraints. If the objective function f_0 is convex, the constraints can only be expressed as *less than or equal to* a constant [15, p. 127]. That is how it is expressed in Eq. (2.22). Sometimes it could be desirable to set up the problem with a *greater than or equal to* constraint, for

example when the power pattern is to be optimized to a certain shape defined by a mask. If an upper and a lower mask of the power pattern is given, a constraint such as

$$\text{lower mask} \leq \text{power pattern} \leq \text{upper mask}$$

would be preferred. The left inequality here does not correspond to a convex constraint. Unfourtunately, the solution close at hand, that is to change the constraint to

$$\text{lower mask} \geq -\text{power pattern},$$

is not acceptable for convex optimization either. The reason for this is that changing the sign of a convex function would turn it into a concave function. Hence, the constraint is still not allowable for convex optimization.

Owing to the fact that this setup is not convex, another problem formulation must be made. In the optimizations performed in this report, this was solved by turning the objective function into the distance between the power pattern and the desired shape, instead of the power pattern itself. Due to the power pattern being linearized as previously described, such a distance would constitute a convex objective function. The optimization can then be performed with the constraint

$$\text{distance between linearized power pattern and mask} \leq \text{value to be minimized.}$$

More details on this are also presented in Section 3.3.

Convex optimization has in conclusion several advantages, but also some disadvantages that need to be taken care of when defining a solvable problem.

3

Methods

In the introduction, a short summary of three different methods from previous studies was presented. One method used an iterative norm minimization technique, one used convex optimization and the third was a deterministic approach based on a density taper technique. The latter two are the ones further studied in this report and are described in greater detail later in this chapter. The first method however, is shortly described forthwith together with the reasons for why it is disregarded in this thesis.

3.1 Expansion on Previous Studies

The iterative norm minimization technique presented in [3–5] is based on Compressive Sensing. Letting the starting point of the problem be a dense array with closely spaced elements simulating a continuous source distribution, a regularization can be applied to the antenna weights in the minimization problem. The regularization takes the form of two norms, the L_1 and the L_∞ norm. The minimization of the L_1 norm promotes sparsity, while minimizing the L_∞ norm limits the range of its components and forces them to get stuck to either end of the range, thus promoting uniform amplitude for some weights. The method allows for isophoric solutions with elements having the same phase by solving

$$\min_{0\leq\mathbf{w}\leq 1} ||\mathbf{w}||_1 + \gamma||\mathbf{w} - \alpha||_\infty \qquad \text{subject to power pattern constraints} \tag{3.1}$$

where $\mathbf{w}$ is a vector containing the weights of all elements. The parameter γ controls the influence of the two norms, and thereby the tradeoff between sparsity and binarity in the solution. The scalar α represents the half value of the uniform amplitude wanted in the solution. Minimizing the expression will compel the weights to stick to either 0 or 2α.

The method is improved by iteratively removing active elements from the dense array. This increased sparsity in the solution is promoted by introducing a diagonal weighting matrix $\mathbf{Z}^k$ which penalizes elements with a small amplitude. This is done by solving the following problem in each iteration k:

$$\min_{\mathbf{w}^k} ||\mathbf{Z}^k\mathbf{w}^k||_1 + \gamma||\mathbf{w}^k - \alpha||_\infty \qquad \text{subject to power patterns constraints,} \tag{3.2}$$

with

$$\begin{cases} \mathbf{Z}_{n,n}^{k} = \left(\left|w_n^{k-1}\right| + \delta\right)^{-1} \\ \mathbf{Z}_{n,p}^{k} = 0 \quad \text{if} \quad n \neq p. \end{cases} \tag{3.3}$$

Here $\delta > 0$ guarantees that the algorithm is numerically stable. This minimization problem is then solved until no more excitations become zero.

Preliminary results using the iterative norm minimization technique points to great difficulties finding the parameters γ and α. The method is unable to fulfill a satisfactory solution while meeting both inter-element distance demands and uniform amplitude constraints. A suitable weighting between the L_1 and the L_∞ norms was not found. The resulting element positions were either not sparse enough or had varying amplitudes. Furthermore, choosing a static value for α was not possible without a priori knowledge of the resulting array. Instead, α was made an optimization variable and included into the optimization problem. However, this method amendment did not manage to yield satisfactory results.

3.2 General Problem Setup

The two different methods that have been used and examined in the project are henceforth presented. First, the two separate problems to be solved are introduced. They differ slightly between the pencil beam and shaped beam cases. For the case of a pencil beam the sidelobes of the power pattern are to be minimized in the region not belonging to the main lobe. Such an optimization problem can be described as

$$\min_{\mathbf{x}} \max_{u \in u_{SL}} |AF_{\mathbf{x}}(u)|^2 \tag{3.4}$$

where $\mathbf{x} = (x_1, ..., x_N)$ is the element position vector and u_{SL} denotes the u-coordinates in the sidelobe region.

For the shaped beams, the target function differs from the previous case. Here, the difference between the desired power pattern and the synthesized power pattern is to be minimized in the main lobe region. In other words, the ripple is minimized. In the rest of the visible region there are sidelobes which are bounded upward by a predetermined sidelobe level, $SLL_{\max}$. Given a reference power pattern $|h(u)|^2$ the optimization problem can be mathematically described as

$$\begin{aligned} &\min_{\mathbf{x},\boldsymbol{\Delta\Phi}} \max_{u \in u_{SB}} \left| |AF_{\mathbf{x},\boldsymbol{\Delta\Phi}}(u)|^2 - |h(u)|^2 \right| \\ &\text{subject to} \quad \max_{u \in u_{SL}} |AF_{\mathbf{x},\boldsymbol{\Delta\Phi}}(u)|^2 \leq SLL_{\max} \end{aligned} \tag{3.5}$$

where $\boldsymbol{\Delta\Phi} = (\Delta\Phi_1, ..., \Delta\Phi_N)$ is the phase shift vector, u_{SB} is the u-coordinate in the shaped beam region and $|AF_{\mathbf{x},\boldsymbol{\Delta\Phi}}(u)|^2$ is the produced power pattern.

Both optimization problems are also subject to an inter-element distance constraint on $\mathbf{x}$. The general isophoric constraint is mathematically modelled by $|w_n| = \text{const}$, $\forall\, n = 1, ..., N$. The main difference between the two optimization problems, is as

mentioned, that the target function changes from minimizing the SLL to minimizing the distance from a given power pattern mask. As can be seen from these optimization problems, the definition of the mask is an integral part of the problem definition.

Referring to Section 2.2, the problems described are both complicated, non-convex optimization problems with a large number of local minima. In the remainder of this chapter, two methods are proposed for counteracting this problem. The first method is an iterative linearization and convex optimization, while the second method is based on a deterministic selection of optimization starting positions and phases.

3.3 Convex Optimization Method

In this section a method performing iterative convexification is presented. The problem formulations are presented mathematically and are throughout this project solved using the MATLAB package CVX [16].

3.3.1 Pencil Beam Synthesis

A one-dimensional antenna array with N elements is considered. The goal is to find the optimal positions of these elements in order to obtain a pencil beam power pattern with minimum SLL, while the elements are excited with uniform amplitude and in this case also uniform phase.

In [6], a method for the optimization of isophoric antenna arrays for the synthesis of pencil beam patterns according to Eq. (3.4) is presented. The method is based on an iterative procedure where convex optimization is implemented in order to minimize the maximum SLL by finding the optimal positions of a fixed number of elements. For the case of a linear array in [6], the elements are first placed equally spaced with the spacing $d = 0.5$, where d is given in λ. This is a non-sparse array, and consequently further development of the method is necessary in order to obtain sparse arrays. However, the idea behind the optimization performed in [6] can be used both to find the lowest SLL for a filled array, as well as to find the minimum number of elements that produces a pencil beam pattern with a predetermined SLL. Such a development of the method is presented henceforth.

In brief, the developed method is based on an iterative algorithm which optimizes the positions of a given number of elements, N. In order to only find the lowest possible SLL for a given N, the algorithm is only performed once. If the goal instead is to find the minimum N able to fulfill a predetermined maximum SLL, the algorithm is performed several times for different N. The minimum N fulfilling the requirements is then determined. The choice of N in each iteration of the algorithm is based on a form of binary search presented later.

Examining the algorithm in [6] for solving the problem given in Eq. (3.4) is done by first explaining one iteration k. The weights in Eq. (2.6) are taken to be $w_n = 1/N$

for all n, hence the array is excited with uniform amplitude. In each iteration a displacement δ_n^k of the position x_n^k of each element is determined according to

$$x_n^k = x_n^{k-1} + \delta_n^k, \qquad \text{for} \qquad n = 1, ..., N$$

However, such a minimization problem, where the optimization variable δ_n^k is in an exponent, is not convex. In order to make it convex, a Taylor expansion can be used provided that the displacement δ_n^k is small. The Taylor expansion $e^{j\beta} \approx 1 + j\beta$ yields the following approximated array factor at iteration k:

$$AF_{\delta_n^k}^k(u) = \frac{1}{N}\sum_{n=1}^{N} e^{j2\pi u(x_n^{k-1}+\delta_n^k)} \approx \frac{1}{N}\sum_{n=1}^{N} e^{j2\pi u x_n^{k-1}}(1 + j2\pi u\delta_n^k). \tag{3.6}$$

This linearization with respect to the optimization variable δ_n makes convex optimization possible.

The convex optimization problem to be solved at iteration k is now given by

$$\min_{\boldsymbol{\delta}^k} \rho \quad \text{subject to} \begin{cases} \max\limits_{i=\{1,...,M_u\}} |AF_{\boldsymbol{\delta}^k}^k(u_i)| \leq \rho, \\ |\delta_n^k| \leq \alpha^k, \quad n = 1, ..., N, \\ |x_n^k| \leq L/2 \end{cases} \tag{3.7}$$

where $\boldsymbol{\delta} = (\delta_1, ..., \delta_N)$ is the N-dimensional displacement vector, ρ is an optimization variable and u_i is one of M_u sample points in the sidelobe region. Note that it is the square root of the power pattern that is minimized here. This will yield the same optimal positions since the SLL is still minimized. The purpose of the parameter α^k is to ensure that the Taylor expansion is a good approximation. In [6], $\alpha^k = 0.16, \forall k$, is considered to be a good choice and this value is used throughout all convex optimizations. The last constraint is used in order for the positions to not exceed the antenna length L. The half is required since the positions are centered around $x = 0$. A minimum distance $\delta_{\min} = 0.4$, between two adjacent positions x_n^k and x_{n+1}^k may also be required in the additional constraint

$$|x_{n+1} + \delta_{n+1} - (x_n + \delta_n)| \geq \delta_{\min}.$$

The problem (3.7) is solved iteratively according to the following steps:

1. For $k = 1$ an equi-spaced array is initialized. The initial positions are determined from a given antenna length, L. The spacing is therefore given by $d = L/(N-1)$ and the positions are centered around $x = 0$. This is different from the method in [6] where the spacing $d = 0.5$ determines the antenna length L, instead of the other way around.
2. For $k \geq 1$, the problem (3.7) is solved to produce the displacements δ_n^k.
3. The element positions are updated according to $x_n^k = x_n^{k-1} + \delta_n^k$.
4. Steps 2 and 3 are repeated until $|\rho^{k-1}/\rho^k - 1| \leq 10^{-5}$, that is when the maximum SLL has stopped decreasing.

The presented iterative algorithm will lead to a minimum of the maximum SLL ρ by optimizing the positions of N elements. In order to find the minimum number of elements that manage to push the maximum sidelobe level below a certain limit, ρ_{lim}, a form of binary search is performed. This gives rise to the necessary assumption that the SLL ρ depends on the number of elements N in a non-increasing manner. The assumption has been shown to hold by empirical examination, even if a few values of N do behave contradictory, see Figure 3.1. Nevertheless, the time saved with this approach compared to trying all possible N motivates its use.

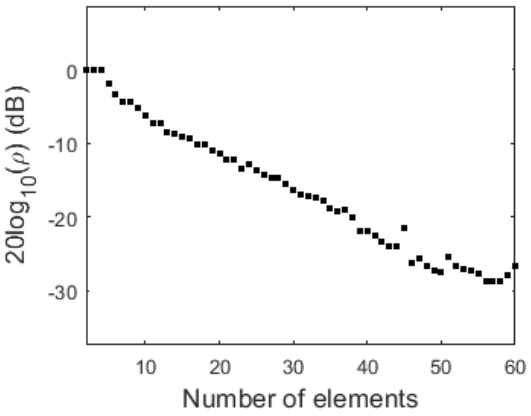

Figure 3.1: The minimized values of the maximum of ρ with respect to the number of elements. Here, the filled antenna is 20λ long, and has 40 elements. The most interesting part of the figure is for element numbers below 40. It can be seen that in this region the dependence is *almost* completely non-increasing.

With the assumption of a non-increasing dependence of ρ with respect to N, the binary search algorithm is executed in the following way. It is assumed that the target N is in the interval $N \in [2, cL]$ for $2 \leq c \leq 3$. This choice of c opens up for the possibility that the number of elements does not have to be lower than the number of elements for the case of a filled array which contains $2L$ elements. In order to find the lowest possible N the following algorithm is implemented:

1. Let $l = 2$ and $r = cL$.
2. Let $N = \text{floor}\left(\frac{l+r}{2}\right)$.
3. Perform the iterative algorithm that finds the minimum of the maximum sidelobe level ρ.
   - If $\rho > \rho_{\text{lim}}$, set $l = N + 1$, and repeat from step 2.
   - If $\rho < \rho_{\text{lim}} - \Delta\rho_{\text{lim}}$, set $r = N - 1$, and repeat from step 2.
   - If $\rho_{\text{lim}} - \Delta\rho_{\text{lim}} \leq \rho \leq \rho_{\text{lim}}$, the minimum number of elements is considered to be found. Return N together with its optimal positions, x_n for $n = 1, ..., N$.

Here $\Delta\rho_{\text{lim}}$ defines the size of the region below ρ_{lim} in which the requirement is considered to be fulfilled. This is necessary due to the improbability that the minimized ρ will become exactly ρ_{lim}. Therefore, it is not possible to anticipate the value of ρ with greater accuracy than what is defined by this interval.

3.3.2 Shaped Beam Synthesis with Phase Tapering

In the previous section, a method for the synthesis of pencil beam patterns was presented. The only optimization variables there were the element positions. Here, an expansion of that method is presented, where the phase is also utilized in order to shape the main lobe into a cosecant squared beam or a flat-top beam. The phase is a free variable without constraints, as opposed to the element positions.

In order for this optimization problem to be convex, a linearization similar to Eq. (3.6) is done. This time, both the element positions x_n, and the phase shifts $\Delta\Phi_n$ are used as optimization variables. In each iteration k these two variables are changed by the small amounts δ_n^k and ϵ_n^k respectively, according to

$$x_n = x_n^{k-1} + \delta_n^k \qquad \text{and} \qquad \Delta\Phi_n^k = \Delta\Phi_n^{k-1} + \epsilon_n^k.$$

A Taylor expansion is done as in the previous section in order to make the optimization problem convex. The final approximated array factor then becomes:

$$\begin{aligned} AF_{\delta_n^k,\epsilon_n^k}^k(u) &= \frac{1}{N}\sum_{n=1}^{N} e^{j(2\pi u x_n^k + \Delta\Phi_n^k)} \approx \frac{1}{N}\sum_{n=1}^{N} e^{j2\pi u x_n^{k-1}}(1 + j2\pi u\delta_n^k)e^{j\Delta\Phi_n^{k-1}}(1 + j\epsilon_n^k) \\ &\approx \frac{1}{N}\sum_{n=1}^{N} e^{j(2\pi u x_n^{k-1} + \Delta\Phi_n^{k-1})}(1 + j2\pi u\delta_n^k + j\epsilon_n^k). \end{aligned} \tag{3.8}$$

The small quadratic term proportional to $\delta_n^k\epsilon_n^k$ is considered negligible and therefore ignored.

The optimization problem in Eq. (3.5) is not convex. However, it may be approximated into a convex problem by linearizing $|AF(u)|^2$, instead of just the array factor. This is similar to the pencil beam case but somewhat more complicated. The derivation is as follows.

Let $AF_u(x, \Delta\Phi)$ denote the array factor with respect to the position x and phase shift $\Delta\Phi$. If, as previously, the two variables change by the small amounts δ and ϵ, the array factor can be written as

$$AF_u(x + \delta, \Delta\Phi + \epsilon) = AF_u(x, \Delta\Phi) + J(x, \Delta\Phi)(\delta, \epsilon) + \text{higher order terms}, \tag{3.9}$$

where J is the Jacobian. The term with the Jacobian is exactly the linearization of the array factor in Eq. (3.8). However, it is the power pattern that is needed for the optimization. Using the array factor in (3.9), it is given by

$$|AF_u(x + \delta, \Delta\Phi + \epsilon)|^2 = \left[AF_u(x + \delta, \Delta\Phi + \epsilon)\right]^* \left[AF_u(x + \delta, \Delta\Phi + \epsilon)\right]. \tag{3.10}$$

The factors can be linearized separately according to:

$$\begin{aligned} &\left[AF_u(x + \delta,\Delta\Phi + \epsilon)\right]^* \left[AF_u(x + \delta, \Delta\Phi + \epsilon)\right] \\ &\quad = \left[AF_u(x, \Delta\Phi) + J(x, \Delta\Phi)(\delta, \epsilon)\right]^* \left[AF_u(x, \Delta\Phi) + J(x, \Delta\Phi)(\delta, \epsilon)\right] \\ &\quad = AF_u(x, \Delta\Phi)^* AF_u(x, \Delta\Phi) + AF_u(x, \Delta\Phi)^* J(x, \Delta\Phi)(\delta, \epsilon) \\ &\quad + J(x, \Delta\Phi)(\delta, \epsilon)^* AF_u(x, \Delta\Phi) + J(x, \Delta\Phi)(\delta, \epsilon)^* J(x, \Delta\Phi)(\delta, \epsilon). \end{aligned} \tag{3.11}$$

The first term is simply the power pattern in the point $(x, \Delta\Phi)$. The two middle terms can be merged together into $2\,\mathrm{Re}\,(AF_u(x,\Delta\Phi)^* J(x,\Delta\Phi)(\delta,\epsilon))$. The last term is quadratic and is therefore ignored. The linearization of the power pattern is finally given by

$$\begin{aligned} |AF(u)|^2_{\text{approx}} &= |AF_u(x+\delta, \Delta\Phi+\epsilon)|^2 - |AF_u(x,\Delta\Phi)|^2 \\ &= 2\,\mathrm{Re}\,(AF_u(x,\Delta\Phi)^* J(x,\Delta\Phi)(\delta,\epsilon))\,, \end{aligned} \tag{3.12}$$

where $AF_u(x,\Delta\Phi)$ is given after the first equality in (3.8) and $J(x,\Delta\Phi)(\delta,\epsilon)$ is given as the last expression in the same equation.

In order to synthesize a flat-top beam, an optimization setup different from the pencil beam case is needed. The distance between the power pattern $|AF(u)|^2$ and the flat-top level is to be minimized. The flat-top level is taken to be a variable itself, called P_{top}, in order to improve the optimization. Furthermore, the SLL is to be lower than a predetermined value $SLL_{\max}$. Mathematically this problem is expressed as follows:

$$\min_{\boldsymbol{\delta}^k, \boldsymbol{\epsilon}^k, P_{\text{top}}} \gamma \quad \text{subject to} \begin{cases} \left| |AF^k_{\delta^k_n, \epsilon^k_n}(u_i)|^2_{\text{approx}} - P_{\text{top}} \right| \le \gamma, \quad i = 1, ..., N_u \\ \max\limits_{j=\{1,...,M_u\}} |AF^k_{\delta^k_n, \epsilon^k_n}(u_j)| \le \sqrt{P_{\text{top}}}\, 10^{SLL_{\max}/20} \\ |\epsilon^k_n|, |\delta^k_n| \le \alpha^k, \qquad n = 1, ..., N \end{cases} . \tag{3.13}$$

Here the power of 10 is used in order to be able to state $SLL_{\max}$ in decibels, u_i is one of the N_u sample points in the flat-top beam region, and u_j one of the M_u points in the SLL region.

For the cosecant squared beam synthetization, a similar setup is made. Compared to the flat-top case, P_{top} is replaced by the power pattern of the cosecant squared function in the correct region. Again the ripple in the main lobe is minimized according to

$$\min_{\boldsymbol{\delta}^k, \boldsymbol{\epsilon}^k} \gamma \quad \text{subject to} \begin{cases} \left| |AF^k_{\delta^k_n, \epsilon^k_n}(u_i)|^2_{\text{approx}} - G(u_i) \right| \le \gamma, \quad i = 1, ..., N_u \\ \max\limits_{j=\{1,...,M_u\}} |AF^k_{\delta^k_n, \epsilon^k_n}(u_j)| \le 10^{SLL_{\max}}/20 \\ |\epsilon^k_n|, |\delta^k_n| \le \alpha^k, \qquad n = 1, ..., N \end{cases} , \tag{3.14}$$

where $G(u)$ is the function given in Eq. (2.16).

3.4 Deterministic Method

In this section, another method for the optimization of antenna power patterns is presented. It is based on a deterministic approach to obtain suitable starting values for the positions and phase shifts. The starting values can be used in an optimization procedure, for instance the MATLAB function *fminimax*.

3.4.1 Density Taper

In [17], a method for synthesizing isophoric sparse arrays is presented. The deterministic part of the optimization is the so called *density taper* technique. This previously known method for approximating a continuous aperture current distribution with an array of isophoric elements is predictable, hence deterministic. The authors suggest a two step method minimizing the approximation error between a current distribution and approximating array obtained using the density taper technique. In the first step, an analytical solution is found under simplifications which in the second step are removed in order to find a more accurate solution.

The analytical approximation is made by minimizing a cost functional of the difference between the desired far-field

$$f_0(u) = \int_{-a}^{a} h(x) e^{jkux}\, dx, \tag{3.15}$$

where $2a$ is the length of the antenna and the synthesized far-field

$$f_a(u) = \frac{1}{N} \sum_{n=1}^{N} e^{jkux_n} \tag{3.16}$$

in the L_∞-norm. The function $h(x)$ is the complex reference distribution function corresponding to a desired far-field pattern, and is normalized such that

$$\int_{-a}^{a} h(x)\, dx \equiv 1. \tag{3.17}$$

The Taylor distribution in Section 2.1.8 is used as $h(x)$ for obtaining a pencil beam. The cost functional is expressed as

$$\Theta(x_1, x_2, ..., x_n) = \|f_0 - f_a\|_\infty . \tag{3.18}$$

The source Taylor distribution $h(x)$ is partitioned into N segments $(\hat{x}_{n-1}, \hat{x}_n)$ of equal area $1/N$. It follows that minimizing the cost functional in Eq. (3.18) corresponds to

$$\min_{x_n \in (-a,a)} \left| \sum_{n=1}^{N} \left(\int_{\hat{x}_{n-1}}^{\hat{x}_n} h(x) e^{jkux}\, dx - \frac{1}{N} e^{jkux_n} \right) \right| \tag{3.19}$$

over the u-coordinates of interest. By supposing that minimization of Eq. (3.19) is achieved by minimizing each of the summation terms separately, the minimization problem can be written as

$$\min_{x_n \in (\hat{x}_{n-1}, \hat{x}_n)} \left| \int_{\hat{x}_{n-1}}^{\hat{x}_n} h(x) e^{jkux}\, dx - \frac{1}{N} e^{jkux_n} \right|, \qquad n = 1, ..., N. \tag{3.20}$$

The authors state that this separate minimization of N sub-problems can not be proved necessary, but still considered reasonable. For the complete far-fields to be equal, the far-fields from each segment need to be equal as well. By approximating the exponential according to its first Taylor expansion around zero

$$e^{jkux} \approx 1 + jkux, \tag{3.21}$$

assuming

$$k(x - x_n)u \ll 1, \tag{3.22}$$

the minimization of the linearized Eq. (3.20) is ensured if the element positions are chosen according to

$$x_n = N \int_{\hat{x}_{n-1}}^{\hat{x}_n} xh(x)\, dx. \tag{3.23}$$

An interpretation of Eq. (3.23) is that x_n is the barycenter of the interval $(\hat{x}_{n-1}, \hat{x}_n)$ with respect to the density $h(x)$. The assumptions (3.22) stipulates that the solution is accurate when the maximum observation angle and the element spacings are both sufficiently small.

As a way to improve on the simplifications introduced by the Taylor approximation in (3.21), the authors in [17] suggest a second step using the analytical solution as a starting guess for an optimization procedure to minimize the cost functional in Eq. (3.18). The authors argue that the starting values are close enough to the global optimum that local minimization methods can obtain the globally optimal solution. Instead of matching the far-field function, the optimization in the second step could mean minimizing the power pattern difference, the maximum of the SLL or any other optimization target function. This optimization can be performed using the MATLAB function *fminimax*.

In the case of a complex reference source $h(x)$, the method above can be used with the absolute value $|h(x)|$ to obtain positions with the density taper method, and then choosing the phase of $h(x_n)$ corresponding to the calculated positions [18].

3.4.2 Arbitrary Reference Source

Using the deterministic method in Section 3.4 to produce a shaped beam requires a suitable reference source $h(x)$. Reference sources can be described by the complex element weights w_n in an array factor. Calculating a reference source for a specific power pattern is a two step process.

The first step is to determine the complex element weights in an array factor corresponding to the desired power pattern of the shaped beam. This is done by synthesizing the desired power pattern for a filled antenna array with uniform element spacing. Defining the power pattern mask and using *fminimax* to perform the optimization, element amplitudes and phase shifts can be obtained. The optimized amplitudes and phase shifts w_n, represent the reference function $h(x)$. Since the reference function is used to determine element positions in the density taper technique, there are no constraints on uniform amplitude in this optimization.

As described in Section 2.1.3, different array factors can produce the same unique power pattern. The second step of the process is to use the optimized weights to obtain equivalent weights and array factors producing the desired power pattern as described in Section 2.1.3. Among the available options, a set of weights are selected based on a decided criteria. For instance, it could be the reference source with the

most uniform amplitude. A uniform amplitude results in the largest minimum inter-element distances using a density taper technique as in the deterministic method.

The selected reference source is then interpolated using FFT interpolation in order to increase the resolution of the complex source. The interpolated reference source can be used in the deterministic method to produce optimization starting values.

4

Implementation and Assessment of Results

In this chapter, results from the implementation of the two described methods are presented and discussed. A more detailed description of the realization of the methods is provided when needed. The chapter is concluded with a more general discussion of the results, together with an exposition of possible future extensions. Furthermore, the results of the optimized positions and phase shifts are presented in Appendix A.

To highlight different aspects of the methods, they have been implemented for five different cases. The cases, which are presented below, are selected to demonstrate both the usability and the varying solution performance provided by the methods:

Case 1. Pencil beam with minimum SLL
Case 2. Pencil beam with maximum sparsity
Case 3. Shaped beam with cosecant squared pattern
Case 4. Shaped beam with flat-top pattern
Case 5. Reconfigurable beam

The fifth case seeks to synthesize an antenna array able to transmit two different beams: a shaped beam and a pencil beam. The reconfiguration between the two beam patterns is performed with only a change in the applied phase shift. The antenna positions remain the same.

For simplicity of comparing the different cases, the same antenna size of 20λ has been used to evaluate all of the cases. A conventional, filled antenna array of that size is considered to have 40 elements due to the physical size of each element. If the elements were infinitesimally small, an inter-element distance of $\lambda/2$ would have resulted in 41 elements.

The pencil beams are synthesized over the interval $u \in [-2, 2]$ to allow for steering, as described in Section 2.1.1. Steering of shaped beams is considered less relevant in practice, and they are therefore only synthesized over the visible region $u \in [-1, 1]$.

4.1 Case 1: Pencil Beam with Minimum SLL

The first case concerns the minimization of the SLL for a filled array. In order to evaluate the results by more than the minimum SLL, two additional measures of performance are specified. They are the HPBW and the directivity. A filled uniform array with no applied phase shifts has a directivity of 16 dB and HPBW of 2.54°. These values are used when comparing to the synthesized beam patterns.

The optimization mask applied around the main lobe has a width of $2.5 \cdot \text{HPBW}$, where the HPBW concerns the filled array. This width was chosen to be slightly wider than the First Null Beam Width (FNBW) which is regularly approximated as $2 \cdot \text{HPBW}$ [8, p. 40]. The width of the main lobe means that the available range of steering is reduced in order for the entire main lobe to be kept inside the visible region. The reduced range of steering is reflected in the applied sidelobe mask by two spans close to $u = \pm 2$ where the SLL is not minimized. The spans are both half as wide as the allowed main lobe width.

4.1.1 Convex Optimization Method

In Figure 4.1, the results obtained using the convex optimization method presented in Section 3.3.1 are shown. With the optimized positions, the antenna manages to reduce the SLL to −20.4 dB. This synthesized beam has a HPBW of 2.66° which is 0.12° wider than that of the uniform array.

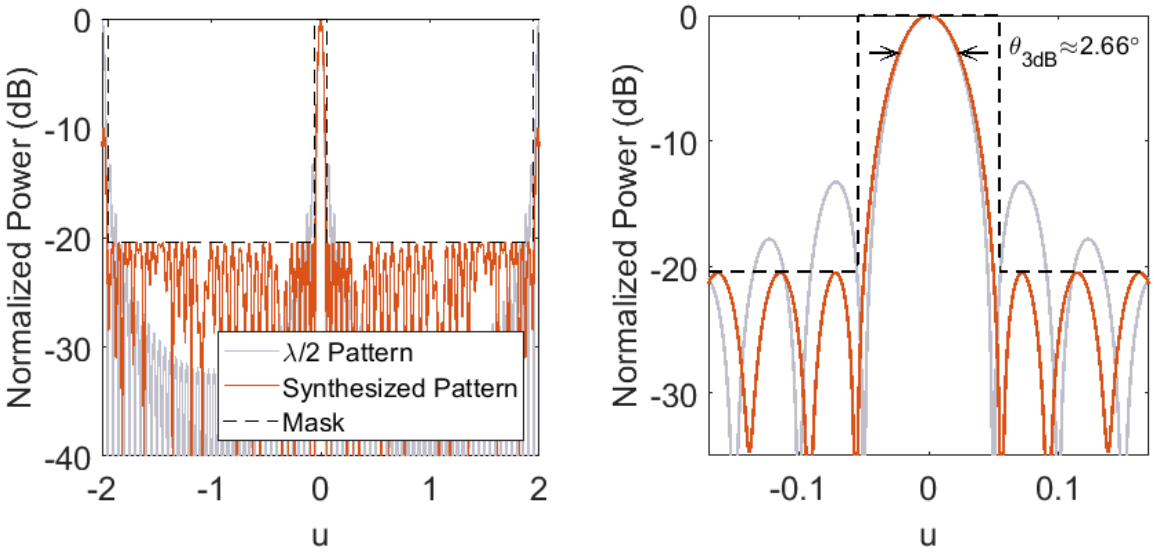

(a) Total beam pattern.

(b) Zoomed in main lobe beam pattern.

Figure 4.1: Convex method: Synthesized pattern normalized to 0 dB from antenna of length 20λ having 40 elements. SLL = −20.4 dB, HPBW = 2.66° and directivity = −0.5 dB compared to the $\lambda/2$ array.

Furthermore, the directivity is decreased by 0.5 dB compared to the uniform array. This directivity difference is a reasonable result since the sidelobes touches the optimized mask over the total range of u. In comparison, the beam pattern from the uniform array goes well below the SLL over a large range of u. This tendency is seen for all of the synthesized beam patterns.

4.1.2 Deterministic Method

The results in Figure 4.2 are obtained using the method described in Section 3.4.1. In order to choose starting positions yielding minimum SLL, a parameter search for different values of $\bar{n}$ and SLL_{Taylor} was performed for the pencil beam optimization. The resulting normalized power pattern was obtained for a Taylor distribution using $\bar{n} = 3$ and $SLL_{\text{Taylor}} = -22.3$ dB as parameters for the MATLAB function *taylorwin*. The SLL achieved was -21.9 dB and the HPBW was 2.77°, that is 0.23° larger than for the $\lambda/2$ array. The directivity of the synthesized array was 0.5 dB lower than for the $\lambda/2$ array.

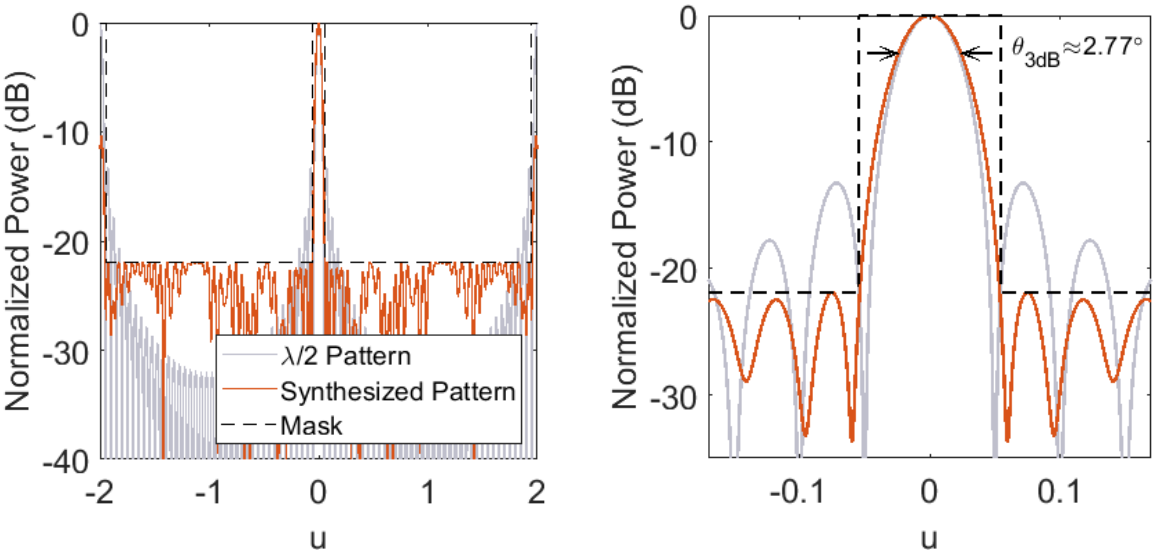

(a) Total beam pattern.

(b) Zoomed in main lobe beam pattern.

Figure 4.2: Deterministic method: Synthesized pattern normalized to 0 dB from antenna of length 20λ having 40 elements. SLL = -21.9 dB, HPBW = 2.77° and directivity = -0.5 dB compared to the $\lambda/2$ array.

Several constraints were applied to the optimization in order to evaluate different setups. Requiring symmetric element positions drastically lowered the performance of the array. The process of obtaining starting positions for the optimization from the density taper on the other hand lowered the SLL by 1.3 dB compared to using uniform starting positions. This points to the problem having many local minima and shows the importance of choosing suitable starting positions for obtaining a satisfactory solution.

Comparing the results of the convex and deterministic methods, it can be seen that the deterministic method achieves 1.5 dB lower SLL and has a 0.11° wider HPBW. The directivity of both methods is the same compared to the $\lambda/2$ array with constant phase. Both methods show considerable benefits from the freedom of positioning the elements in a filled array.

4.2 Case 2: Pencil Beam with Maximum Sparsity

The second case assumes the same mask dimension as in the first case and concerns the minimization of the number of elements needed to achieve a maximum SLL of both −13 dB and −17 dB.

4.2.1 Convex Optimization Method

In Figure 4.3 the results obtained using the convex optimization method with the goal of an SLL at −13 dB. The number of elements resulting in an SLL closest below −13 dB was 24 elements with the corresponding SLL of −13.1 dB. The directivity of this array is 2.4 dB below that of the corresponding filled uniform array with 40 elements. The main cause of this decrease is the reduction of elements which lowers the directivity with 2.2 dB. Concerning the width of the main lobe, the HPBW is slightly smaller than that of the uniform array, more specifically HPBW = 2.47°.

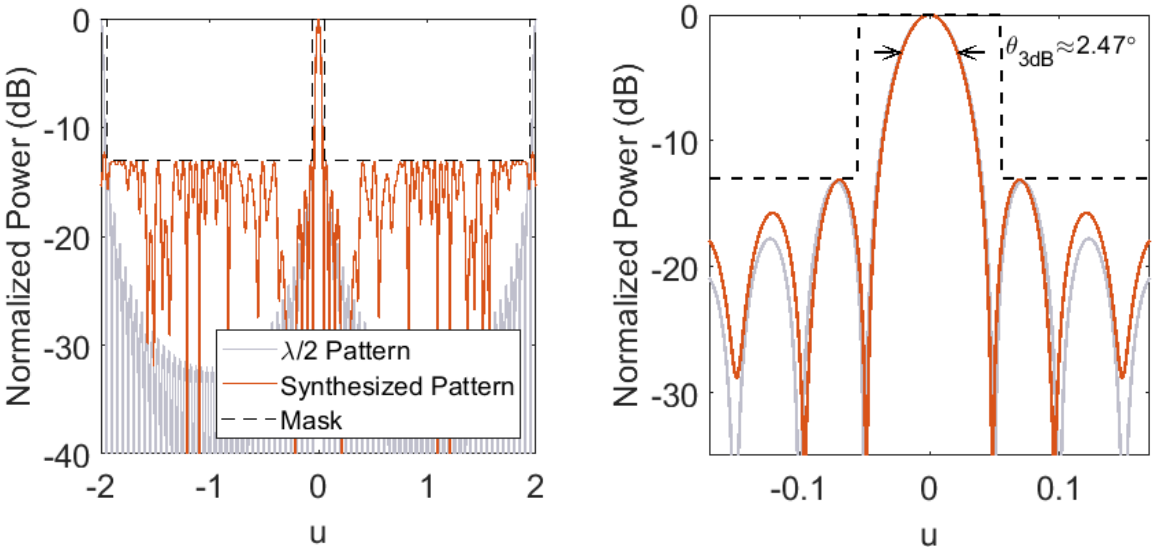

(a) Total beam pattern.

(b) Zoomed in main lobe beam pattern.

Figure 4.3: Convex method: Synthesized pattern normalized to 0 dB from antenna of length 20λ having 24 elements. SLL = −13.1 dB, HPBW = 2.47° and directivity = −2.4 dB compared to the $\lambda/2$ array.

The corresponding beam pattern for an SLL of −17 dB is shown in Figure 4.4. Here, 34 elements was found to be the lowest number of elements, obtaining a maximum SLL of −17.9 dB. The directivity of this beam pattern is 1.0 dB below that of a uniform filled array, of which 0.7 dB comes from the reduction of elements. Furthermore, the synthesized beam has a HPBW of 2.55° which is very close to that of the uniform filled array.

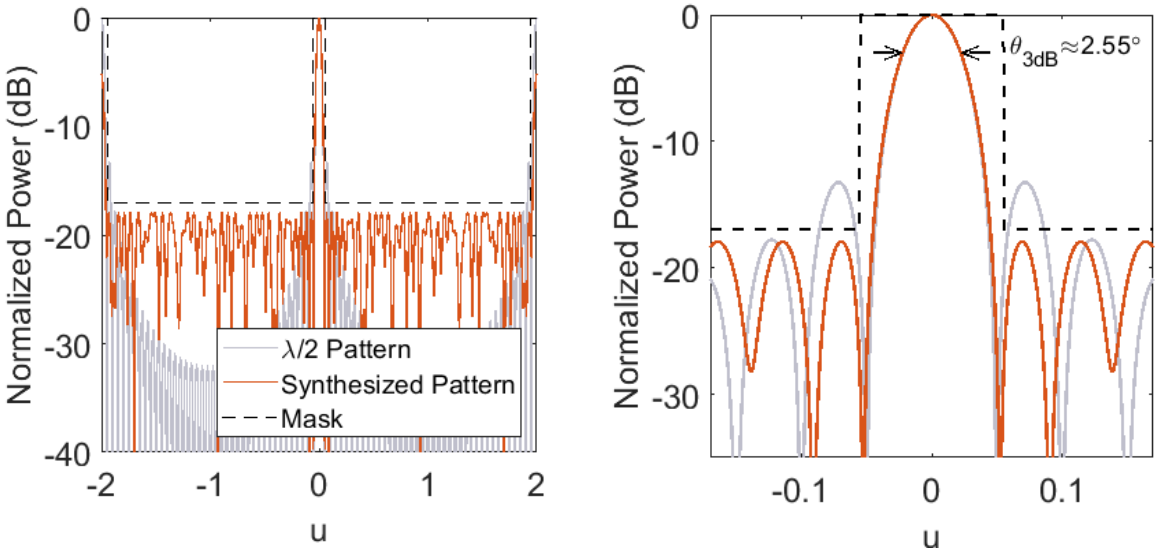

(a) Total beam pattern.

(b) Zoomed in main lobe beam pattern.

Figure 4.4: Convex method: Synthesized pattern normalized to 0 dB from antenna of length 20λ having 34 elements. SLL = −17.9 dB, HPBW = 2.55° and directivity = −1.0 dB compared to the $\lambda/2$ array.

4.2.2 Deterministic Method

To minimize the number of elements for each given SLL, an implementation similar to that of Section 4.1.2 was made. A parameter search over *taylorwin* input values $\bar{n}$ and SLL_{Taylor} was conducted for a decreasing number of elements until an SLL of −13 dB and −17 dB respectively was no longer fulfilled. In this way, the maximally sparse solution was determined.

The resulting power pattern for −13 dB in Figure 4.5 is achieved using 22 elements. The SLL obtained was −13.2 dB using $\bar{n} = 4$ and $SLL_{\text{Taylor}} = -13.7$ dB as inputs for the *taylorwin* function. The directivity of the sparse array is −2.6 dB compared to the $\lambda/2$ array, which is the same as the reduction due to the sparsity. This points to the beam pattern itself being more directive, which is further reinforced by the HPBW of 2.47° being slightly narrower than for the $\lambda/2$ array.

Figure 4.6 presents the beam pattern with an SLL of −17.3 dB which was formed using 30 elements. The parameters for the *taylorwin* function was $\bar{n} = 2$ and

$SLL_{\text{Taylor}} = -17.7\,\text{dB}$. Compared to the filled uniform array, the directivity was $-1.4\,\text{dB}$ of which $-1.2\,\text{dB}$ are due to the element reduction. The HPBW was 2.80°.

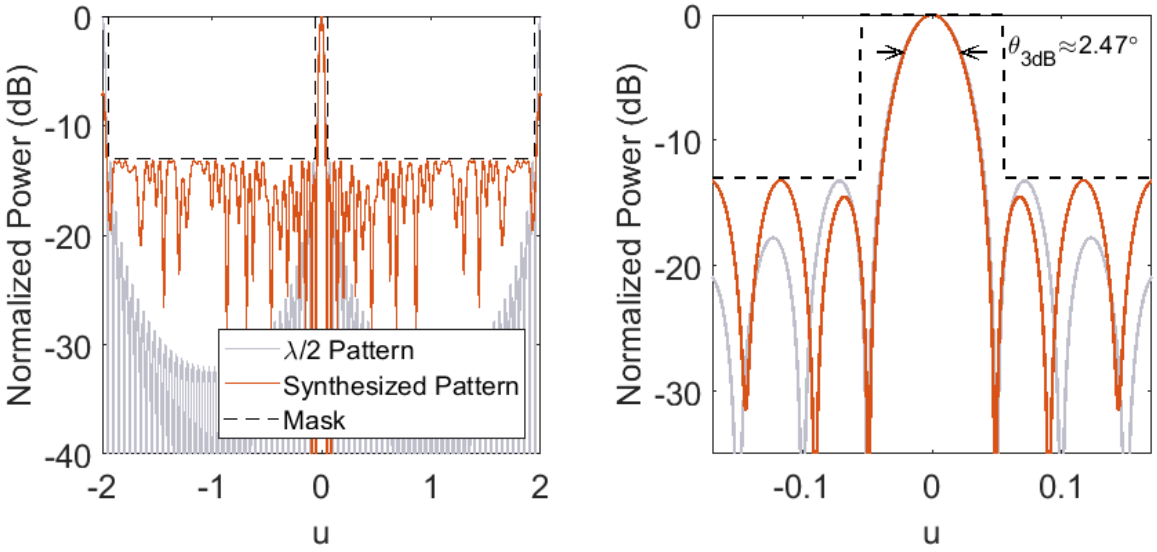

(a) Total beam pattern.

(b) Zoomed in main lobe beam pattern.

Figure 4.5: Deterministic method: Synthesized pattern normalized to 0 dB from antenna of length 20λ having 22 elements. SLL = $-13.2\,\text{dB}$, HPBW = 2.47° and directivity $-2.6\,\text{dB}$ compared to the $\lambda/2$ array.

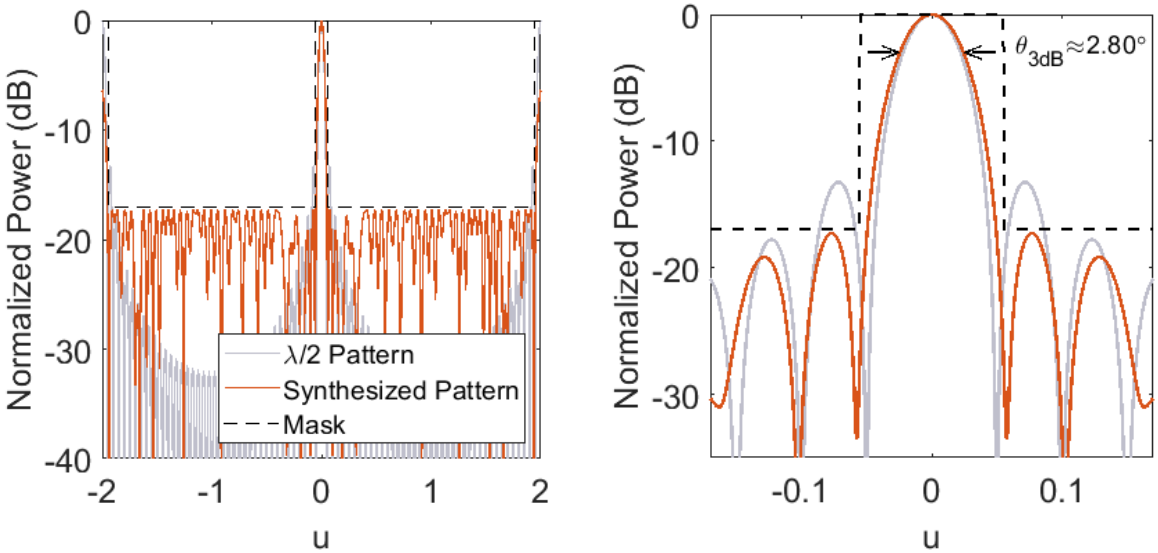

(a) Total beam pattern.

(b) Zoomed in main lobe beam pattern.

Figure 4.6: Deterministic method: Synthesized pattern normalized to 0 dB from antenna of length 20λ having 30 elements. SLL = $-17.3\,\text{dB}$, HPBW = 2.80° and directivity $-1.4\,\text{dB}$ compared to the $\lambda/2$ array.

An interesting observation to make regarding the Taylor distribution and the final beam pattern is that the parameter SLL_{Taylor} is slightly lower than the achieved SLL for both Case 1 and Case 2. This would suggest a rule of thumb for appropriate intervals to search for parameters producing the optimal element positions.

Comparing the results of the convex and determinstic methods it can be seen that the convex method results in two and four additional elements to achieve the desired SLL of $-13\,\text{dB}$ and $-17\,\text{dB}$ respectively. The convex method produces in the $-17\,\text{dB}$ case a solution with $0.6\,\text{dB}$ lower SLL and a HPBW which is $0.25°$ narrower than the deterministic solution. In the $-13\,\text{dB}$ case, the convex solution produces a beam pattern with the same HPBW as the deterministic method but with $0.1\,\text{dB}$ lower SLL. Both methods allow for the introduction of considerable sparsity amongst the elements, while maintaining a pencil beam HPBW close to the $\lambda/2$ array and achieving the set SLL for the mask over $u \in [-2, 2]$.

4.3 Case 3: Shaped Beam Cosecant Squared Pattern

The third case concerns the synthesis of a cosecant squared shaped beam defined in Eq. (2.16). The objective was to minimize the ripple over the cosecant squared lobe, while simultaneously minimizing the SLL. A maximum ripple of $1\,\text{dB}$ was desired. The synthesis was performed using both filled and sparse arrays. The sparse arrays have the same number of elements as the antenna producing a pencil beam with an SLL of $-17\,\text{dB}$ in Case 2, Section 4.2. The cosecant squared mask is applied from the HPBW point up to $45°$ and is thereafter replaced by a constant SLL constraint corresponding to the value of the mask at $45°$ or $u = 1/\sqrt{2}$.

4.3.1 Convex Optimization Method

In Figure 4.7, the result from the convex method with a filled array is shown. It is clear that the ripple at the right half of the cosecant region is unacceptable. This too large ripple makes minimizing the SLL non-rewarding, and therefore $-13\,\text{dB}$ was simply chosen as a mask for negative u. The reason for the large ripple can be explained by the fact that the optimization of the power pattern is done in linear scale, rather than in logarithmic (decibel) scale. A small magnitude ripple in linear scale will correspond to larger changes as the logarithmic values decrease. Hence the ripple is much larger in this scale. This is something that is difficult to address, since optimization in the logarithmic scale would not be a convex problem.

Another dissatisfying matter with the result in Figure 4.7 is that the method does not manage to push down the SLL below the mask to the right of the cosecant squared lobe. Due to the unsatisfactory results for the filled array, no optimization was done for the sparse counterpart.

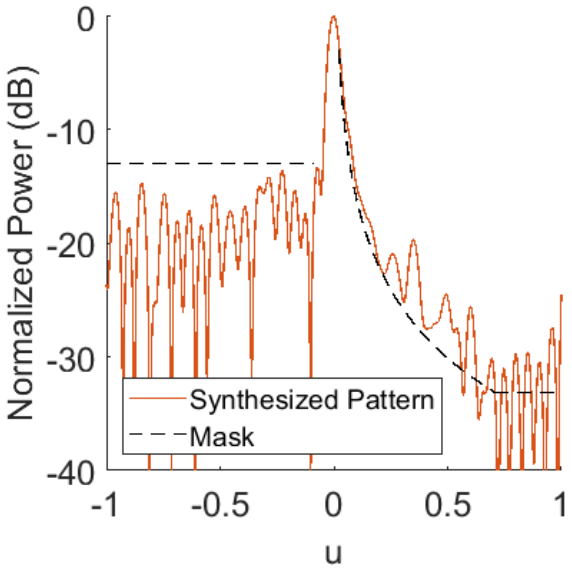

Figure 4.7: Convex method: Synthesized cosecant squared power pattern with 40 elements. SLL for negative u = −13.0 dB.

4.3.2 Deterministic Method

A reference source fulfilling a mask defining the cosecant squared pattern was created using the method described in Section 3.4.2. The initial reference source optimization used starting values with amplitudes one and random phase shifts. The minimized objective function is the ripple over the cosecant squared lobe which ranges from the approximate HPBW position of the pencil beam to 45°. The minimization is performed while fulfilling constraints on the sidelobe regions, defined from $u = -1$ to a distance from the center and from the end of the cosecant squared mask to $u = 1$.

A reference source from the multitude of equivalent options was chosen based on the inter-element distances using the density taper technique. From a random search procedure ranging from one to 60 minutes, the reference source corresponding to the largest minimum distance between elements was selected.

The reference source was then used in the optimization procedure in Section 3.4 to minimize the ripple. Maintaining an acceptable ripple, the optimization was performed for different requirements on the SLL and varying mask dimensions in order to find the minimum SLL. The resulting power patterns for antennas using 40 and 30 elements are seen in Figure 4.8a and 4.8b respectively. For a filled array, the minimum SLL achieved was −21.0 dB resulting in a maximum ripple of 1.0 dB. For the sparse array of 30 elements the minimum SLL achieved was −17.0 dB with a maximum ripple of 1.4 dB.

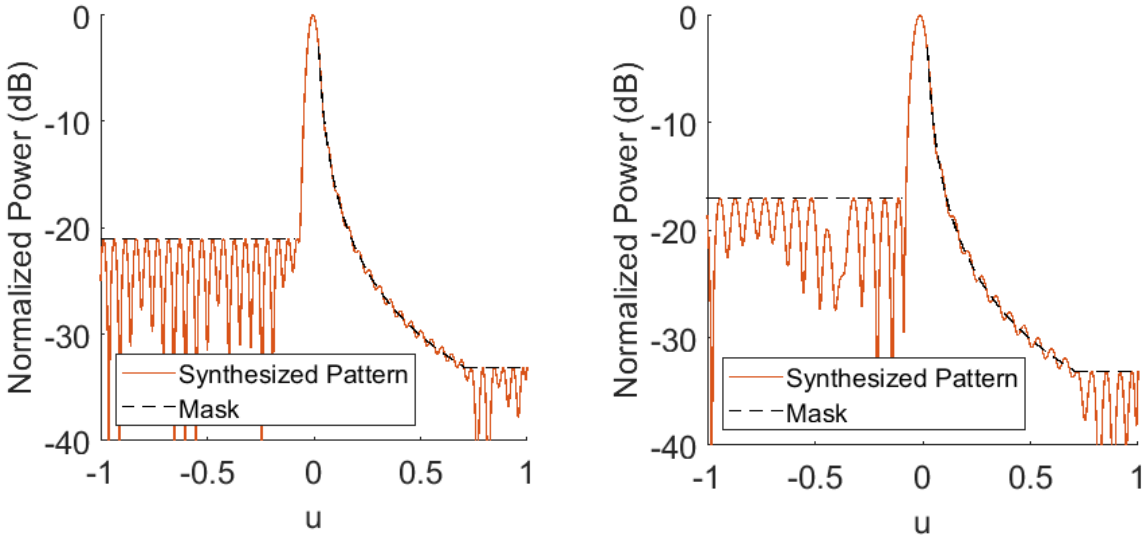

(a) $N = 40$, SLL $= -21.0\,\text{dB}$, ripple $= 1.0\,\text{dB}$

(b) $N = 30$, SLL $= -17.0\,\text{dB}$, ripple $= 1.4\,\text{dB}$

Figure 4.8: Deterministic method: Synthesized cosecant squared power patterns for 40 and 30 elements with minimum SLL.

There are many parameters which affect the final result of the optimization for minimizing the ripple. Adjusting the mask dimensions and SLL can change the optimization result drastically. Slackening of some conditions, for example the distance from the main lobe to the first sidelobe restricted by the mask can improve other parts of the antenna diagram. The changes can be applied both to the creation of the reference source and to the optimization of the isophoric array. The starting positions obtained from the reference source are important for the success of the final optimization. Therefore, a more thorough selection of the reference source, other than a random search, could improve the results significantly. It is however, difficult to define which criteria the reference source should meet in order to yield starting values which produce a better final power pattern. A way to improve on the choice of reference source would be to use a genetic algorithm to aid in the search [11, p. 112]. Using a complex density taper approach as described in [7] also has potential to improve the results by providing different starting positions to the optimization. To a large extent, the limiting constraint seems to be the required inter-element distance of 0.4λ which hinders the placement of the elements in their optimal positions.

4.4 Case 4: Shaped Beam Flat-top Pattern

The fourth case aims for a flat-top lobe with a beam width of 30°. Again, the objective was to minimize the ripple over the flat-top region and simultaneously minimizing the SLL. The maximum accepted peak-to-peak ripple was 1 dB and the synthesis was performed both for a filled and a sparse array. The sparse array

contains the same number of elements as the resulting antenna in Case 2, Section 4.2.

4.4.1 Convex Optimization Method

In Figure 4.9 the results from the convex method are shown, both for the filled array in Figure 4.9a and for the sparse array with 34 elements in Figure 4.9b. The convex method performs better for this case compared to the cosecant squared beam synthesis in the previous section. The reason for this is that the desired level of the top of the main lobe in this case is constant. This implies that it does not matter whether the optimization is done in linear or logarithmic scale. The relative deviation of the synthesized beam from the desired level will have the same order of magnitude over the full main lobe region. For the filled and sparse arrays, the minimized SLL becomes $-14.2\,\mathrm{dB}$ and $-13.0\,\mathrm{dB}$ respectively. During the optimization it turned out that the synthesized beam pattern was extremely dependent on the precise mask dimensions, and the SLL could differ by several decibels from only minor variations. The presented results are the ones which fulfill the lowest SLL for all $u \in [-1, 1]$.

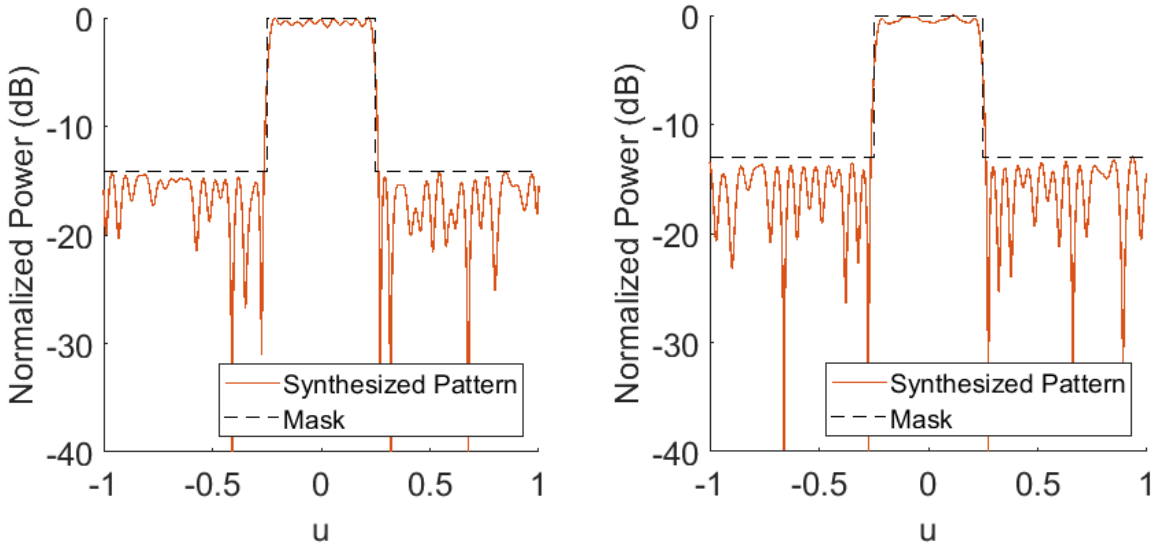

(a) $N = 40$, SLL $= -14.2\,\mathrm{dB}$, ripple $= 0.9\,\mathrm{dB}$

(b) $N = 34$, SLL $= -13.0\,\mathrm{dB}$, ripple $= 0.8\,\mathrm{dB}$

Figure 4.9: Convex method: Synthesized flat-top power patterns for 40 and 34 elements with minimum SLL.

4.4.2 Deterministic Method

A mask for the flat-top beam was created and a corresponding complex reference source obtained in a similar way to Case 3. The reference source was used in the optimization minimizing the ripple in the flat top region of the beam. The

minimization was conditioned on fulfilling the SLL constraint over $u \in [-1, 1]$ and the inter-element distance constraint.

Performing the optimization for different values of the SLL resulted in satisfactory ripple of 0.9 dB for both the filled and the sparse array. The two arrays achieved an SLL of -21.0 dB and -20.0 dB respectively. The power patterns are presented in Figure 4.10.

As in Case 3, the adjustment of the mask SLL and spacing from the ends of the flat-top beam to the sidelobe region have a large impact on the optimization result. This requires careful adjustment to the specific case in order to achieve a desired outcome.

An interesting observation to make is that the SLL is only increased by 1.0 dB for the same ripple when the array is made sparse. There might be several reasons for the small decrease in performance when the number of elements is reduced by 25 %. One reason could be that the 0.4λ inter-element distance constraint stops the elements from positioning closely in accordance with the density taper technique. When decreasing the number of elements, a position density similar to the reference source could be achieved while fulfilling the element-to-element distance constraint. With the distance constraint, a larger number of elements is not guaranteed to achieve a better result. The grouping of the elements can be seen in the position plot in Figure A.9, where many of the elements are positioned as close together as the constraint allows.

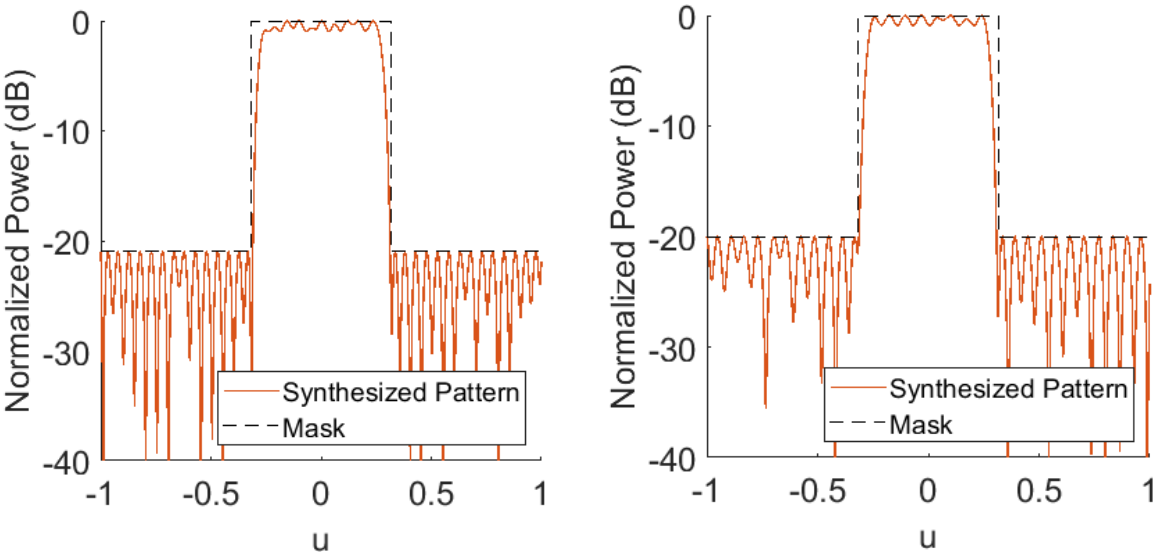

(a) $N = 40$, SLL $= -21.0$ dB, ripple $= 0.9$ dB

(b) $N = 30$, SLL $= -20.0$ dB, ripple $= 0.9$ dB

Figure 4.10: Deterministic method: Synthesized flat-top power patterns of width 30° for 40 and 30 elements with minimum SLL.

4.5 Case 5: Reconfigurable beam

The fifth case concerns the switching between a pencil beam and a shaped beam by applying different phase shifts to the same antenna array. The reconfigurable beams are produced for both a cosecant shaped beam and a flat-top beam. Shapes of the main beams are the same as in Case 3 and 4. The optimizations are performed for both a filled array and a sparse array, where the sparse array has the same number of elements as in Case 2.

4.5.1 Convex Optimization Method

To begin with, because of the unsatisfactory results from synthesizing a cosecant squared beam pattern with the convex method, such a reconfigurable beam was not synthesized with this method.

Instead, reconfigurable arrays were only optimized for flat-top beams with the convex optimization method. Due to the difficulties of synthesizing flat-top beam patterns with the convex method in Case 4, no new flat-top beams were produced in this case to avoid the increased complexity of ensuring reconfigurability. Instead, the antenna arrays produced in Case 4 are reused and a new phase is optimized independently for a pencil beam with the given positions.

In Figure 4.11a, the optimized pencil beam is presented together with the corresponding flat-top beam for 40 elements, and in Figure 4.11b for 34 elements. It turned out that by using the optimized positions from Case 4 a good pencil beam could still be synthesized by only optimizing the phase. For the filled array, the pencil beam has a HPBW of 2.84° and for the case with 34 elements 2.86°.

A basis for the method to produce a reconfigurable beam is that the optimization of positions and phases for the shaped beam is performed before the optimization of phases for the pencil beam. This leaves twice as many degrees of freedom for the shaped beam compared to the pencil beam. The reason for this is that a pencil beam is more easily formed than a shaped beam. Consider the constant inverse Fourier transform of an ideal pencil beam, a Dirac delta function, which is a constant unity. This would suggest that the main condition for creating a pencil beam is a uniform distribution from the elements over the length of the antenna. The likeliness of creating a more uniform-like distribution from positions optimized for a shaped beam is higher than the opposite. This approach is the opposite of the one detailed in [19], where a shaped beam is based on pencil beam positions.

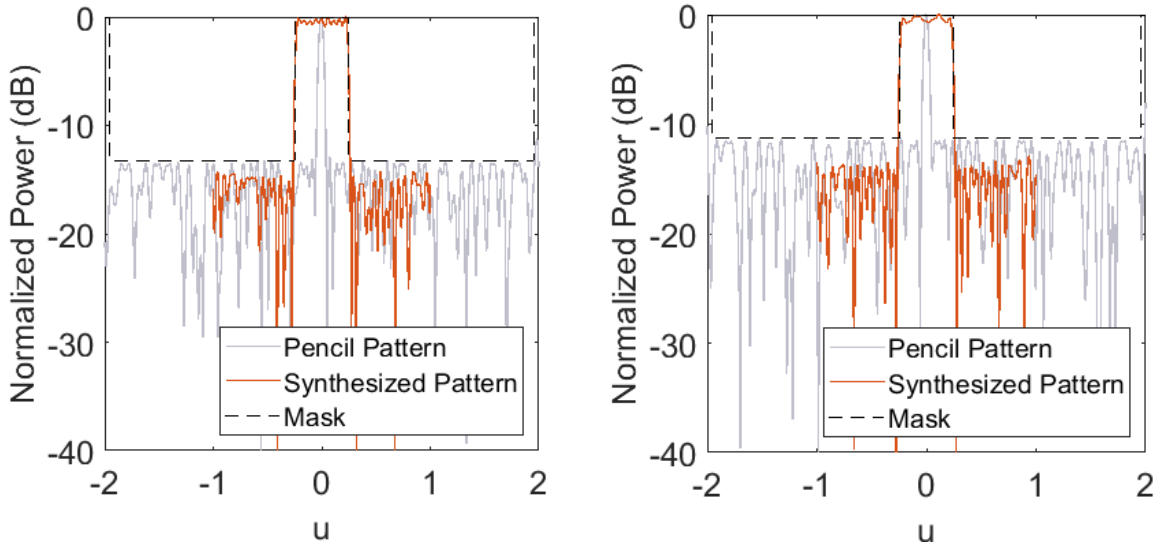

(a) $N = 40$, $\mathrm{SLL}_{\mathrm{shaped}} = -14.2\,\mathrm{dB}$, $\mathrm{SLL}_{\mathrm{pencil}} = -13.2\,\mathrm{dB}$, $\mathrm{HPBW} = 2.84°$

(b) $N = 34$, $\mathrm{SLL}_{\mathrm{shaped}} = -13.0\,\mathrm{dB}$, $\mathrm{SLL}_{\mathrm{pencil}} = -11.3\,\mathrm{dB}$, $\mathrm{HPBW} = 2.86°$

Figure 4.11: Convex method: Synthesized reconfigurable flat-top power patterns normalized to 0 dB for 40 and 34 elements.

4.5.2 Deterministic Method

When it comes to the reconfigurability between a shaped beam and a pencil beam, the method is varied slightly compared to Case 3 and 4. The method for obtaining the reference source remains the same as for the previous cases, but two additions are made to the final optimization in order to also produce a pencil beam. The first change is the introduction of a new constraint. The constraint sets an SLL requirement on the beam obtained from the element positions without phase shift. The second change is the addition of a new optimization function following the minimization of the shaped beam ripple. The goal is to produce a pencil beam by optimizing the phase for the fixed element positions. A mask similar to that in Case 1 and 2 is used, and it covers $u \in [-2, 2]$, unlike the first optimization of the shaped beam which is as previously performed for $u \in [-1, 1]$.

With the deterministic approach, an additional optimization goal was to achieve a similar SLL with both the shaped beam and the pencil beam. This resulted in a worsening SLL for both the shaped beam and the pencil beam compared to the previous cases when they were produced independently. The filled array and the sparse array having 30 elements were evaluated for both reconfigurable beams, and the resulting power patterns are presented in Figure 4.12 and Figure 4.13.

The cosecant reconfigurable beam in Figure 4.12 achieved an SLL of $-19.0\,\mathrm{dB}$ when having 40 elements. The accompanying pencil beam has an SLL of $-19.0\,\mathrm{dB}$. The maximum ripple in the cosecant beam is 0.7 dB and the pencil beam HPBW is 2.85°. For the array of 30 elements, the cosecant beam had an SLL of $-16.0\,\mathrm{dB}$ while the

pencil beam achieved −16.6 dB. The maximum ripple is 1.0 dB and the pencil beam HPBW is 3.62°.

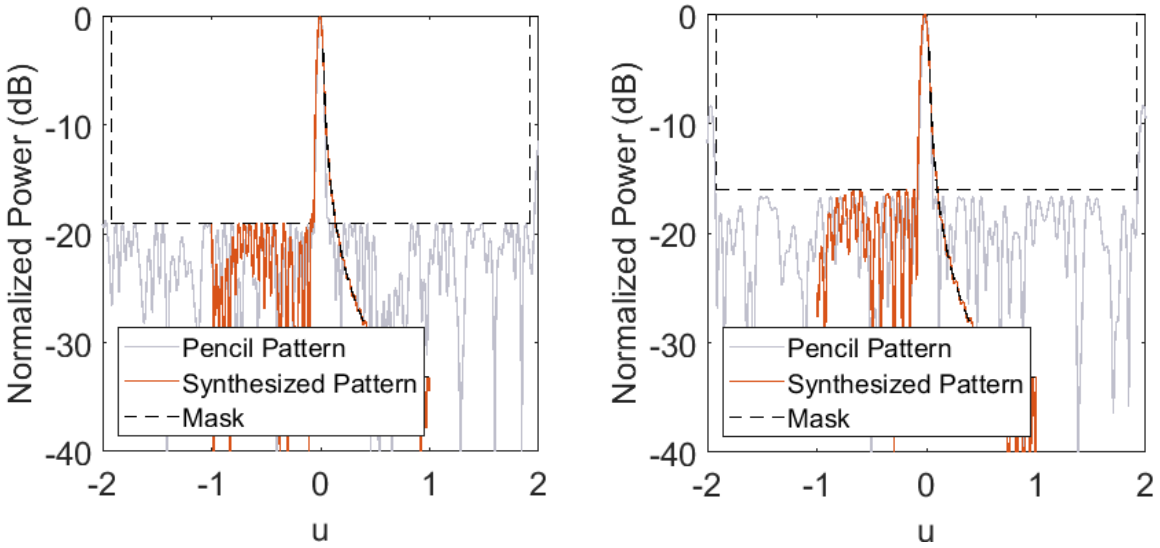

(a) $N = 40$, $\mathrm{SLL}_{\mathrm{shaped}} = -19.0\,\mathrm{dB}$, $\mathrm{SLL}_{\mathrm{pencil}} = -19.0\,\mathrm{dB}$, ripple =0.7 dB, HPBW = 2.85°

(b) $N = 30$, $\mathrm{SLL}_{\mathrm{shaped}} = -16.0\,\mathrm{dB}$, $\mathrm{SLL}_{\mathrm{pencil}} = -16.6\,\mathrm{dB}$, ripple = 1.0 dB, HPBW = 3.62°

Figure 4.12: Deterministic method: Synthesized reconfigurable cosecant squared and pencil power patterns normalized to 0 dB for 40 and 30 elements with minimum common SLL.

The flat-top reconfigurable beam, in Figure 4.13 achieved for the filled array a SLL of −18 dB with a ripple of 0.8 dB. The accompanying pencil beam obtained a SLL of −18.3 dB and a HPBW of 3.14°. The sparse array achieved a SLL of −16.5 dB with a ripple of 1.0 dB. The pencil beam had a SLL of −17.0 dB and a HPBW of 3.77°.

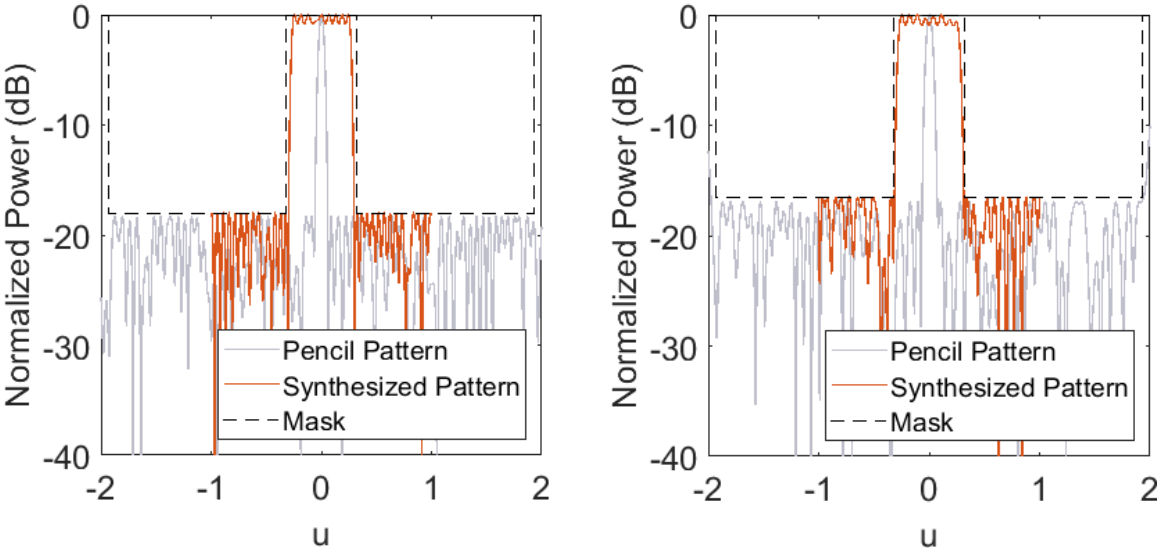

(a) $N = 40$, $\mathrm{SLL}_{\mathrm{shaped}} = -18.0\,\mathrm{dB}$, $\mathrm{SLL}_{\mathrm{pencil}} = -18.3\,\mathrm{dB}$, ripple $= 0.8\,\mathrm{dB}$, HPBW $= 3.14°$

(b) $N = 30$, $\mathrm{SLL}_{\mathrm{shaped}} = -16.5\,\mathrm{dB}$, $\mathrm{SLL}_{\mathrm{pencil}} = -17.0\,\mathrm{dB}$, ripple $= 1.0\,\mathrm{dB}$, HPBW $= 3.77°$

Figure 4.13: Deterministic method: Synthesized reconfigurable flat-top and pencil power patterns normalized to 0 dB for 40 and 30 elements with minimum common SLL.

4.6 Pencil Beam Steering

To demonstrate the pencil beam steering possibilities arising from enforcing the SLL over the mask for $u \in [-2, 2]$ an example is presented for a sparse and uniform amplitude array. The reconfigurable pencil beam obtained in Figure 4.13b is steered to an angle of $\theta_s = 60°$. The applied phase shift for steering is calculated according to Eq. (2.3) and added to the existing phase shift. Steering the pencil beam represents a translation of the power pattern in the u-coordinate, which can be seen in Figure 4.14. It can also be observed that the SLL remains the same in the visible region $u \in [-1, 1]$ while larger sidelobes occur outside of the visible region, as expected.

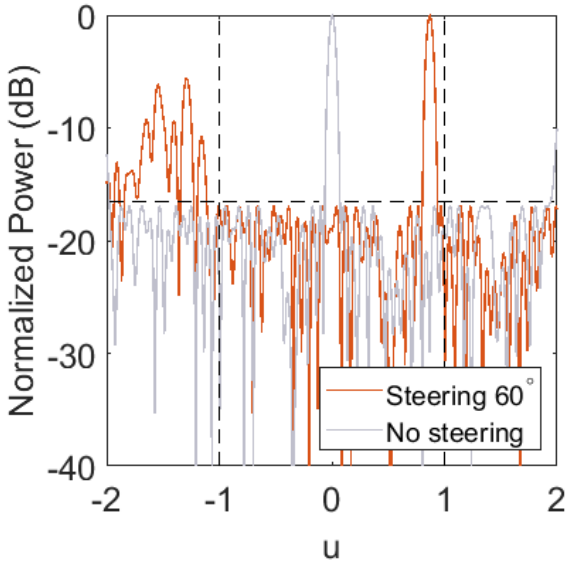

Figure 4.14: Steering to 60° of the flat-top reconfigurable pencil beam synthesized using the deterministic method with 30 elements.

4.7 General Discussion

To begin with, the implementation results show that both pencil and shaped beams can be synthesized with sparse isophoric antenna arrays and still meet mask requirements. Reconfigurability between a shaped beam and a pencil beam is shown possible with only a small decrease in SLL compared to the individually optimized antennas.

From the methods and corresponding results, some general observations about both the convex and the deterministic method can be made. A common factor is that the precise dimensions of the target power pattern mask greatly affect the optimization results. Mask dimensions include, but are not exclusive to: the width of the main lobe region, the width of the separation between the main and sidelobe regions and for the shaped beams, the exact region where the ripple is minimized. In this way the mask dimensions can also be viewed as variables to adjust in order to produce a satisfactory power pattern. This creates in effect another optimization problem intertwined with the original optimization problem. The solution of this combined problem would be massively complicated.

The results show that the deterministic approach yields power patterns with better performance than the convex approach. This is mainly seen in the generally lower SLL produced with the deterministic method. A reason for this can be due to how the optimization problem is set up. While the MATLAB function *fminimax* allows for the use of mask values in logarithmic scale and all types of inequality and equality constraints, the convex requirement makes the optimization to a mask considerably more difficult. For the problem to remain convex, the objective function can not be expressed using logarithmic terms. This poses complications due the importance of

relative power levels in the problems. The difficulties presented by this limitation can be seen in the cosecant squared beam pattern shown in Figure 4.7 where the ripple increases with decreasing normalized power level. All functions not originally convex also need to be linearized with respect to the optimization variables, which makes the optimization problem an approximation of the original problem. The deterministic method on the other hand, optimizes the exact objective function. The above factors all contribute to increasing the difficulty of posing the convex optimization problem compared to using the *fminimax* function.

From the presented methods and results it is clear that the original optimization problems have a large number of local minima resulting from the large number of degrees of freedom. Local optimization procedures such as *fminimax* are easily trapped in local minima. This means that starting values based on a deterministic approach can provide a considerable advantage because of their expected vicinity to the global minima. Another way to avoid the problem with local minima is to convexify the optimization problem and use convex optimization to reach the global minima. This was done in the convex optimization method, where a global minimum of the approximation is found in each iteration of the iterative procedure. Thus, it is not guaranteed that it is the real global minimum of the original problem that is found. However, the approximation was found to be very close to the original problem, making it probable that the global solution is found anyway. Regardless, a local solution will still constitute a solution which may be worthwhile.

An additional interesting outcome is that the deterministic approach in general does not exploit the total antenna length for the placement of the elements, see the position results figures in Appendix A. The reason for this is due to the different initial positions of the elements in the two methods. In the convex method they are uniformly distributed over the total antenna length in the beginning, while for the deterministic approach they are distributed according to the density taper. The density taper technique means the elements will never be positioned at the outermost ends of the antenna. Since there is likely a minimum close to the starting positions, the elements are not likely to use the full length of the antenna.

The attentive reader will have noticed that the pencil beam optimization in Case 1 and 2 only uses positions as optimization variables. This is an intentional move by the authors. Small scale testing suggests that the introduction of phase optimization does little to improve results. This could in large be due to pencil beams being easily formed from a uniform distribution of the elements over the antenna aperture. The optimization of positions alone is in itself an interesting problem which might offer a deeper insight into the underlying synthesis problem itself. In the next section, further recommendations for future developments of the method are discussed.

4.8 Recommended Future Extensions

Concerning the convex optimization method, there are other ways to implement it for these types of problems, which was indicated in the beginning of this thesis. One

problem with the chosen approach proved to be that the optimization is performed in logarithmic scale, rather than linear scale, as appointed previously. An interesting development of the method would therefore be to enable an optimization in linear scale, for example by linearizing the logarithm of the power pattern, rather than the power pattern in linear scale. Such a linearization would possibly improve the problems with the large differences in ripple for the cosecant squared case.

In order to further evaluate and possibly improve the performance of the deterministic method, there are two evident approaches that can be implemented. The first is the use of a genetic algorithm in the selection of reference source from the 2^M options obtained by applying the technique in Section 2.1.3. Because of the very large number of options, it is not feasible to evaluate all reference sources individually. Introducing a more refined algorithm would therefore increase the possibility of finding a more suitable reference source compared to the random search technique used in the report. In addition, the fitness criteria of the reference source could be adjusted to incorporate for instance smoothness of phase transitions between elements. Due to mutual coupling, large phase differentials between adjacent elements are unpractical to realize. The mutual coupling could make the amplitude even out over nearby elements.

The second possibility of method improvement concerns the density taper technique. In [7], a generalized density taper technique based directly on a complex reference source is derived. The complex density taper technique provides positions and phases not following the same patterns as the density taper technique used in the thesis, which would provide new possibilities to improve the optimization results. Implementation into the given method would be straightforward, as the density taper function is a separate entity and could simply be replaced by another version.

Additional areas of interest to examine would be the stability of the solutions. Introducing a standard deviation variation of the positions and phase shifts and comparing the power patterns would give an indication to how a physically manufactured solution would behave. This would also result in tolerance values to compare to those in the manufacturing process. Investigating the physical behaviour of a manufactured antenna would mean introducing element factors for the antennas and a model for mutual coupling.

5

Conclusion

The purpose of this thesis was to perform a method evaluation for the synthesis of sparse antenna arrays. The first conclusion is that synthesis of antenna arrays with different beam patterns using only the positions and phases is a difficult problem. This fact is confirmed not only by the method evaluation presented in this thesis, but also from the numerous previously published articles in the field. A large number of different methods have been evaluated during the last few decades for this very purpose, and still it is unclear which method is most suitable. The main reason for this would be the large number of degrees of freedom in the problem.

The implementation results of the methods show the feasibility of synthesizing sparse arrays with uniform amplitude excitations and a minimum element-to-element distance. For example, for the pencil beam with an SLL of $-17\,\mathrm{dB}$ the number of elements is reduced from 40, to 30 and 34 elements for the deterministic and convex method, respectively. The main lobe width is largely maintained. This results imply the possibilities of reducing the number of elements and thus making antenna arrays sparse. The results also show the potential of synthesizing reconfigurable sparse antenna arrays, since arrays with the same element positions could transmit both a pencil beam and a shaped beam by applying different phase shifts. For example, a sparse flat-top beam of width 30° and an SLL of $-16.5\,\mathrm{dB}$ was made reconfigurable to a pencil beam with SLL of $-17.0\,\mathrm{dB}$ using 30 elements.

Ultimately, the results suggest that the deterministic method presented in this report is the more apt method for synthesizing sparse isophoric antenna arrays. One of the main reasons for this seems to be the more permissive setup of the optimization problem. The MATLAB function *fminimax* handles a variety of constraints and objective functions, thus allowing the problem to be directly described by a minimization of the distance to a power pattern mask. The convex method conversely limits the functions and constraints that can be used, and therefore makes the optimization problem more difficult to formulate.

Bibliography

[1] O. M. Bucci, T. Isernia, S. Perna, and D. Pinchera, "Isophoric Sparse Arrays Ensuring Global Coverage in Satellite Communications," *IEEE Transactions on Antennas and Propagation*, vol. 62, no. 4, pp. 1607–1618, 2014.

[2] R. J. Mailloux, *Phased Array Antenna Handbook*. Norwood, MA: Artech House, Inc, 2 ed., 2005.

[3] B. Fuchs and S. Rondineau, "Array Pattern Synthesis with Excitation Control via Norm Minimization," *IEEE Transactions on Antennas and Propagation*, vol. 64, pp. 4228–4234, 10 2016.

[4] C. Bencivenni, *Aperiodic Array Synthesis for Telecommunications*. PhD thesis, Chalmers University of Technology, Gothenburg, 2017.

[5] C. Bencivenni, M. V. Ivashina, R. Maaskant, and J. Wettergren, "Synthesis of Maximally Sparse Arrays Using Compressive Sensing and Full-Wave Analysis for Global Earth Coverage Applications," *IEEE Transactions on Antennas and Propagation*, vol. 64, 11 2016.

[6] B. Fuchs, A. Skrivervik, and J. R. Mosig, "Synthesis of Uniform Amplitude Focused Beam Arrays," *IEEE Antennas and Wireless Propagation Letters*, vol. 11, pp. 1178–1181, 2012.

[7] O. M. Bucci, T. Isernia, and A. F. Morabito, "An Effective Deterministic Procedure for the Synthesis of Shaped Beams by Means of Uniform-Amplitude Linear Sparse Arrays," *IEEE Transactions on Antennas and Propagation*, vol. 61, 1 2013.

[8] C. A. Balanis, *Antenna Theory - Analysis and Design*. Hoboken, New Jersey: John Wiley and Sons, Inc., 4 ed., 2016.

[9] P.-S. Kildal, *Foundations of Antenna Engineering : A Unified Approach for Line-Of-Sight And Multipath*. Kildal, 2015.

[10] J. L. Volakis, *Antenna Engineering Handbook*. McGraw-Hill, 4 ed., 2007.

[11] T. Isernia, O. Bucci, and N. Fiorentino, "Shaped Beam Antenna Synthesis Problems: Feasibility Criteria and New Strategies," *Journal of Electromagnetic Waves and Applications*, vol. 12, 1 1998.

[12] A. F. Morabito, A. Massa, P. Rocca, and T. Isernia, "An Effective Approach to the Synthesis of Phase-Only Reconfigurable Linear Arrays," *IEEE Transactions on Antennas and Propagation*, vol. 60, 8 2012.

[13] ITU-R, "Mathematical models for radiodetermination radar systems antenna patterns for use in interference analyses M Series Mobile, radiodetermination, amateur and related satellite services," tech. rep., 2018.

[14] T. T. Taylor, "Design of Line-Source Antennas for Narrow Beamwidth and Low Side Lobes," *IRE Transactions - Antennas and Propagation*, vol. AP-3, pp. 16–28, 1 1955.

[15] S. P. Boyd and L. Vandenberghe, *Convex Optimization*. Cambridge University Press, 2004.

[16] CVX Research Inc., "CVX: Matlab Software for Disciplined Convex Programming," 8 2012.

[17] O. M. Bucci, M. D'Urso, T. Isernia, P. Angeletti, and G. Toso, "Deterministic synthesis of uniform amplitude sparse arrays via new density taper techniques," *IEEE Transactions on Antennas and Propagation*, vol. 58, pp. 1949–1958, 6 2010.

[18] O. M. Bucci, T. Isernia, A. F. Morabito, S. Perna, and D. Pinchera, "On the optimal synthesis of shaped beam sparse arrays having uniform amplitude excitations," in *2010 IEEE International Symposium on Phased Array Systems and Technology*, IEEE, 10 2010.

[19] A. F. Morabito, T. Isernia, and L. Di Donato, "Optimal Synthesis of Phase-Only Reconfigurable Linear Sparse Arrays Having Uniform-Amplitude Excitations," *Progress In Electromagnetics Research*, vol. 124, 2012.

A

Element Positions and Phases

In this Appendix, the values of element positions and phases generating the power patterns in the results are presented both in figures and in tables.

A.1 Case 1: Pencil Beam with Minimum SLL

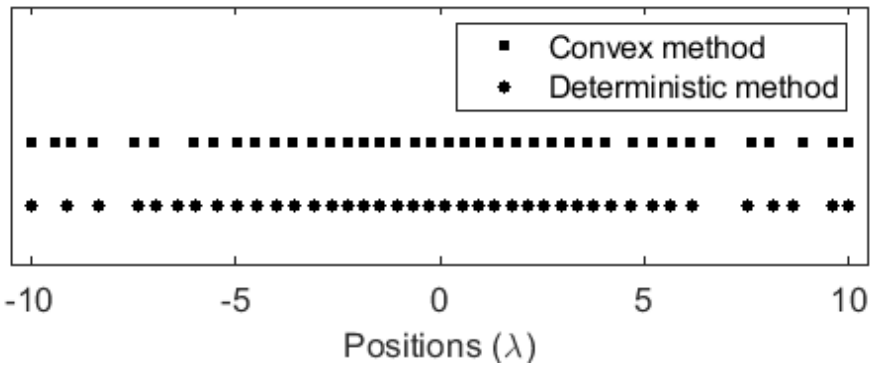

Figure A.1: Element positions for both the convex and deterministic method.

Table A.1: Convex method: Element positions.

N	x_n (λ)	N	x_n (λ)
1	-10.0000	21	0.1993
2	-9.4050	22	0.6147
3	-9.0043	23	1.0147
4	-8.4779	24	1.4147
5	-7.4634	25	1.8673
6	-7.0088	26	2.2746
7	-6.0032	27	2.7444
8	-5.5445	28	3.1676
9	-4.9774	29	3.6069
10	-4.5067	30	4.0265
11	-4.0324	31	4.7128
12	-3.6245	32	5.2205
13	-3.1118	33	5.6643
14	-2.6665	34	6.1057
15	-2.2665	35	6.5964
16	-1.8665	36	7.6164
17	-1.4665	37	8.0393
18	-1.0651	38	8.8752
19	-0.6007	39	9.6000
20	-0.2007	40	10.0000

Table A.2: Deterministic method: Element positions.

N	x_n (λ)	N	x_n (λ)
1	-10.0000	21	0.1431
2	-9.1379	22	0.5431
3	-8.3373	23	0.9431
4	-7.3664	24	1.3431
5	-6.9248	25	1.7431
6	-6.4268	26	2.1545
7	-5.9727	27	2.5545
8	-5.4611	28	2.9545
9	-4.9741	29	3.3545
10	-4.4964	30	3.7736
11	-4.0109	31	4.1866
12	-3.5377	32	4.6597
13	-3.0904	33	5.1802
14	-2.6569	34	5.6553
15	-2.2569	35	6.1475
16	-1.8569	36	7.5280
17	-1.4569	37	8.1393
18	-1.0569	38	8.6129
19	-0.6569	39	9.6000
20	-0.2569	40	10.0000

A.2 Case 2: Pencil Beam with Maximum Sparsity

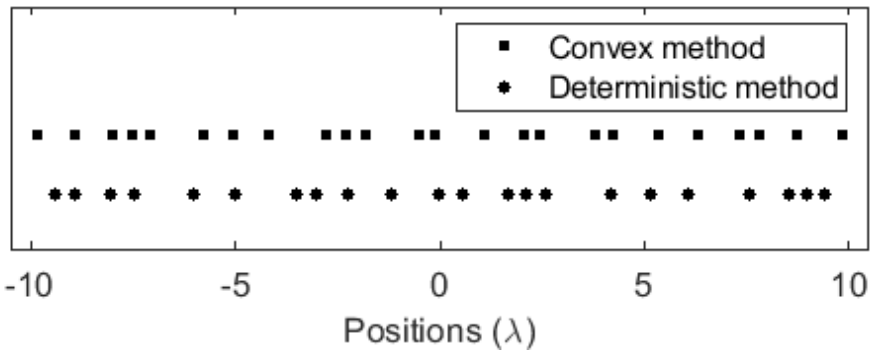

Figure A.2: Element positions for both the convex and deterministic method for SLL $= -13\,\mathrm{dB}$.

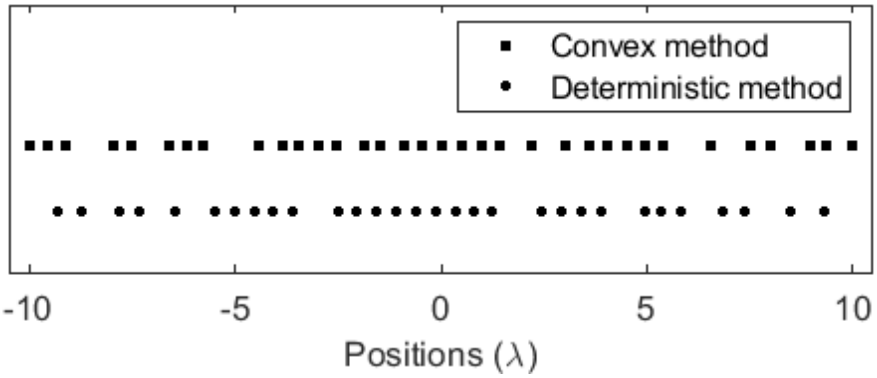

Figure A.3: Element positions for both the convex and deterministic method for SLL = −17 dB.

Table A.3: Convex method: Element positions for SLL = −13 dB.

N	x_n (λ)	N	x_n (λ)
1	-9.8538	13	-0.1228
2	-8.9034	14	1.0763
3	-8.0071	15	2.0570
4	-7.5460	16	2.4584
5	-7.0887	17	3.7819
6	-5.7635	18	4.2422
7	-5.0543	19	5.3695
8	-4.1726	20	6.3032
9	-2.8058	21	7.3299
10	-2.2965	22	7.8296
11	-1.8369	23	8.7299
12	-0.5228	24	9.8538

Table A.4: Convex method: Element positions for SLL = −17 dB.

N	x_n (λ)	N	x_n (λ)
1	-9.9993	18	0.0072
2	-9.5459	19	0.4848
3	-9.1159	20	0.9804
4	-7.9388	21	1.4100
5	-7.5388	22	2.2197
6	-6.6202	23	3.0211
7	-6.1788	24	3.5931
8	-5.7788	25	4.0310
9	-4.4515	26	4.5110
10	-3.8579	27	4.9492
11	-3.4579	28	5.3906
12	-2.9524	29	6.5659
13	-2.5524	30	7.5116
14	-1.8784	31	7.9944
15	-1.4784	32	8.9686
16	-0.9176	33	9.3686
17	-0.4532	34	9.9994

Table A.5: Deterministic method: Element positions for SLL = −13 dB.

N	x_n (λ)	N	x_n (λ)
1	-9.4097	12	0.5647
2	-8.9322	13	1.6898
3	-8.0607	14	2.1222
4	-7.4868	15	2.5945
5	-6.0347	16	4.1942
6	-5.0199	17	5.1619
7	-3.5165	18	6.0920
8	-3.0336	19	7.5529
9	-2.2547	20	8.5496
10	-1.1871	21	8.9931
11	-0.0416	22	9.4097

Table A.6: Deterministic method: Element positions for SLL = −17 dB.

N	x_n (λ)	N	x_n (λ)
1	-9.2915	16	-0.1154
2	-8.7107	17	0.3657
3	-7.7945	18	0.8134
4	-7.3485	19	1.2381
5	-6.4408	20	2.4454
6	-5.4796	21	2.9060
7	-5.0221	22	3.4236
8	-4.5259	23	3.9047
9	-4.0836	24	4.9601
10	-3.6001	25	5.3601
11	-2.4700	26	5.8339
12	-2.0700	27	6.8296
13	-1.5484	28	7.3702
14	-1.0919	29	8.4698
15	-0.6243	30	9.2915

A.3 Case 3: Shaped Beam Cosecant Squared Pattern

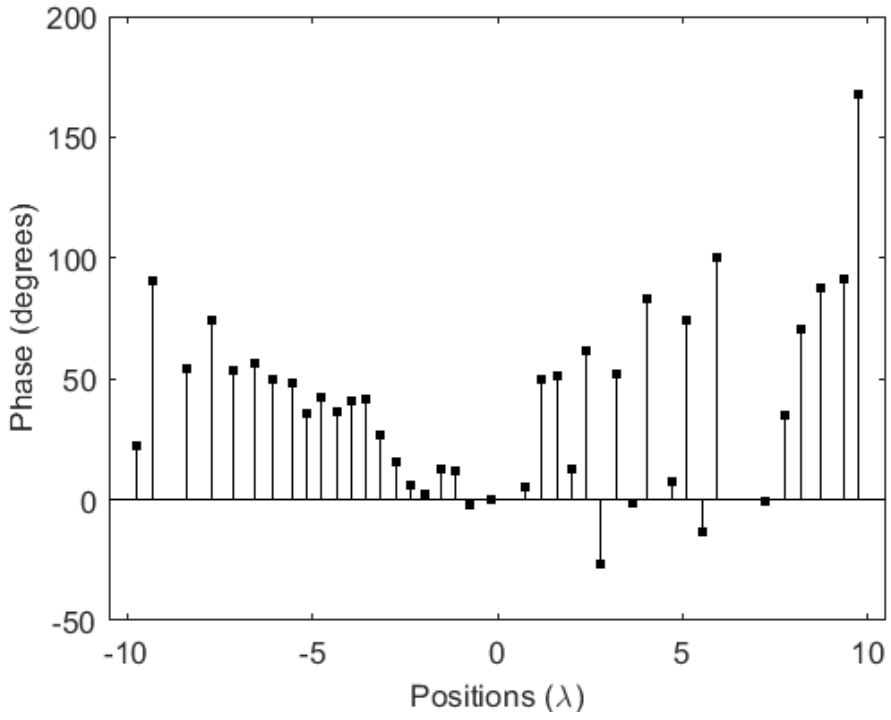

Figure A.4: Convex method: Element positions and phase shifts, $N = 40$, SLL = −13.0 dB.

Table A.7: Convex method: Element positions and phase shifts, $N = 40$, SLL $= -13.0\,\mathrm{dB}$.

n	x_n (λ)	$\Delta\Phi_n$ (degrees)	n	x_n (λ)	$\Delta\Phi_n$ (degrees)
1	-9.7483	22.2037	21	-0.1738	0
2	-9.3385	90.8100	22	0.7399	5.1714
3	-8.3952	54.0204	23	1.2037	49.7210
4	-7.7380	74.5509	24	1.6037	50.9511
5	-7.1264	53.3852	25	2.0037	12.9551
6	-6.5707	56.8098	26	2.4037	61.3126
7	-6.0643	49.9624	27	2.8037	-26.4434
8	-5.5552	48.0189	28	3.2037	52.1529
9	-5.1538	35.9874	29	3.6631	-1.1021
10	-4.7538	42.4209	30	4.0631	83.4861
11	-4.3538	36.6920	31	4.7166	7.7690
12	-3.9538	41.0263	32	5.1166	74.4366
13	-3.5538	41.7813	33	5.5166	-12.9453
14	-3.1538	27.0887	34	5.9166	100.4336
15	-2.7538	15.2961	35	7.2303	-0.3715
16	-2.3538	5.9318	36	7.7876	35.0964
17	-1.9538	2.2560	37	8.1944	70.3114
18	-1.5474	13.0209	38	8.7242	87.6228
19	-1.1394	12.1950	39	9.3483	91.0102
20	-0.7394	-2.1724	40	9.7483	167.6372

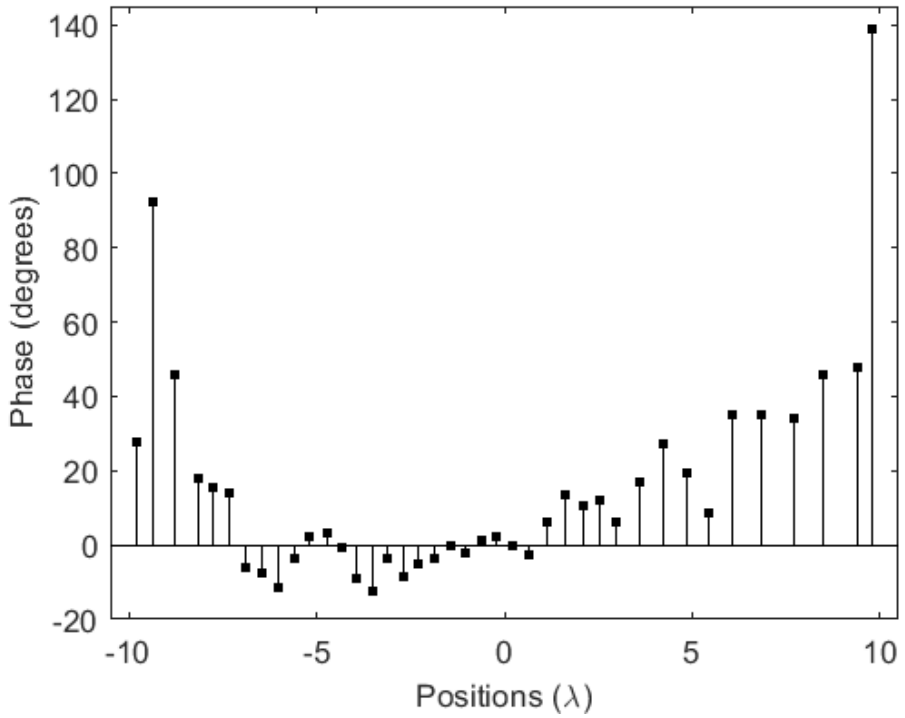

Figure A.5: Deterministic method: Element positions and phase shifts, $N = 40$, SLL $= -21.0\,\mathrm{dB}$.

Table A.8: Deterministic method: Element positions and phase shifts, $N = 40$, SLL $= -21.0$ dB.

n	x_n (λ)	$\Delta\Phi_n$ (degrees)	n	x_n (λ)	$\Delta\Phi_n$ (degrees)
1	-9.8010	27.7399	21	-1.0418	-1.9858
2	-9.3784	92.2907	22	-0.6195	1.2724
3	-8.7952	46.0369	23	-0.2047	2.4532
4	-8.1641	17.9143	24	0.1953	-0.1562
5	-7.7641	15.4192	25	0.6321	-2.8539
6	-7.3180	13.7917	26	1.1241	6.2159
7	-6.9180	-6.0763	27	1.6397	13.3841
8	-6.4648	-7.5663	28	2.0864	10.5150
9	-6.0273	-11.4331	29	2.5338	11.9009
10	-5.5862	-3.5678	30	2.9953	5.9885
11	-5.1862	2.1295	31	3.5846	16.7861
12	-4.7377	3.3800	32	4.2531	27.3818
13	-4.3229	-0.4372	33	4.8588	19.2636
14	-3.9229	-9.0482	34	5.4266	8.4961
15	-3.5229	-12.3668	35	6.0940	35.0819
16	-3.1037	-3.5210	36	6.8429	35.1939
17	-2.7037	-8.2553	37	7.7381	34.2755
18	-2.2840	-4.9661	38	8.4740	45.7681
19	-1.8754	-3.5592	39	9.4010	46.9500
20	-1.4418	0	40	9.8010	138.8443

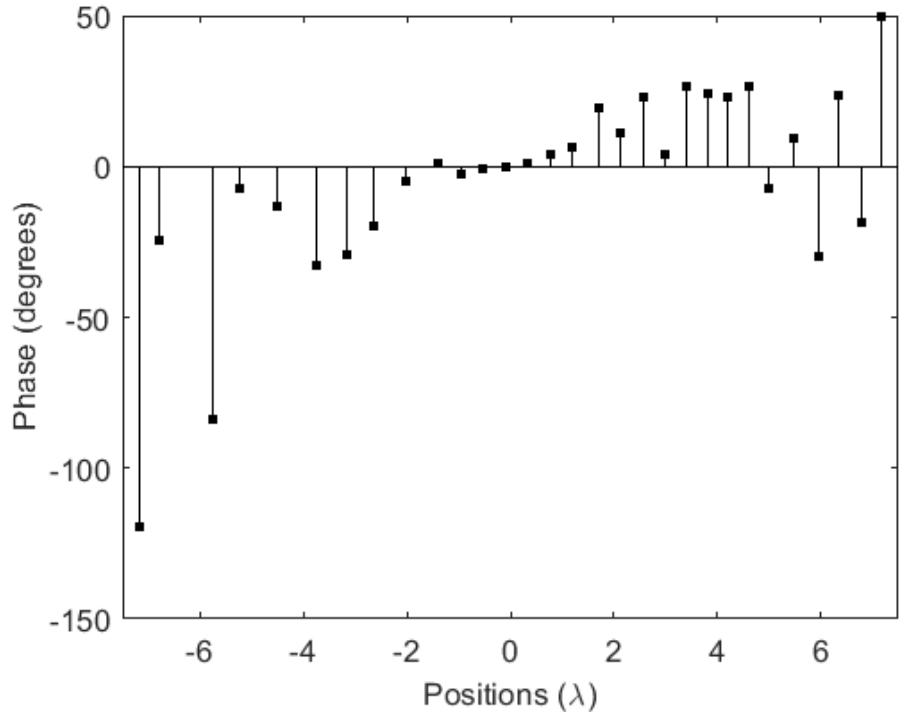

Figure A.6: Deterministic method: Element positions and phase shifts, $N = 30$, SLL $= -17.0\,\mathrm{dB}$.

Table A.9: Deterministic method: Element positions and phase shifts, $N = 30$, SLL $= -17.0\,\mathrm{dB}$.

n	x_n (λ)	$\Delta\Phi_n$ (degrees)	n	x_n (λ)	$\Delta\Phi_n$ (degrees)
1	-7.1835	-119.2068	16	1.2073	6.1490
2	-6.7835	-24.5503	17	1.6979	19.5084
3	-5.7533	-83.9802	18	2.1359	11.2963
4	-5.2421	-7.3825	19	2.5891	22.7129
5	-4.5099	-13.3974	20	2.9891	3.8587
6	-3.7602	-32.4929	21	3.4077	26.7444
7	-3.1627	-29.4838	22	3.8077	23.9104
8	-2.6458	-19.6073	23	4.2077	22.8969
9	-2.0176	-4.7371	24	4.6077	26.3067
10	-1.4108	0.9966	25	5.0077	-7.3762
11	-0.9357	-2.3158	26	5.4629	9.1794
12	-0.5207	-0.6283	27	5.9499	-29.7655
13	-0.0827	0	28	6.3499	23.8499
14	0.3173	1.1883	29	6.7835	-18.5403
15	0.7810	4.2449	30	7.1835	49.4750

A.4 Case 4: Shaped Beam Flat-top Pattern

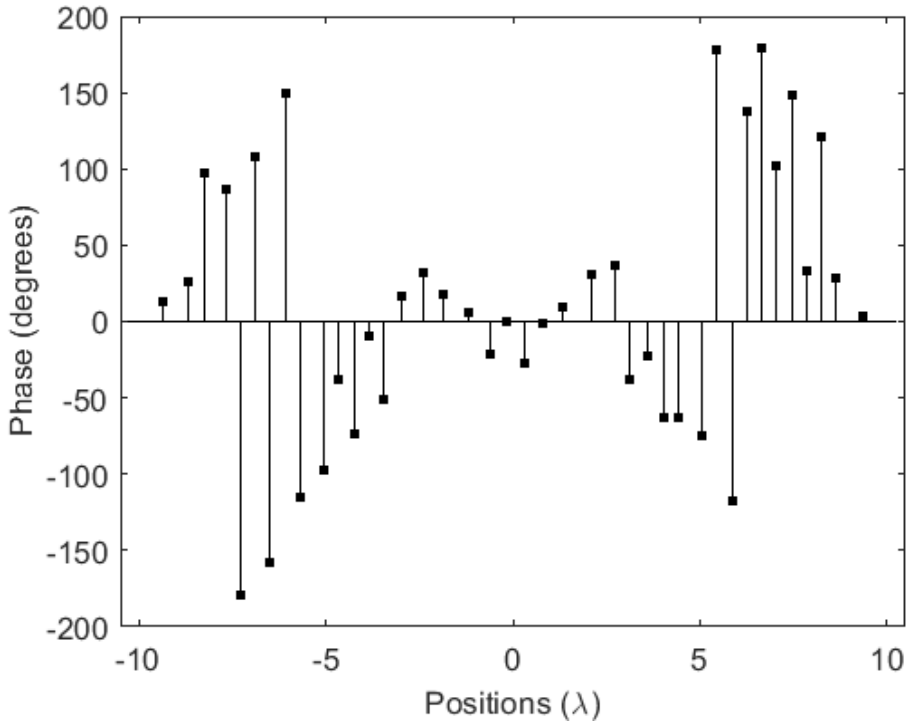

Figure A.7: Convex method: Element positions and phase shifts for the flat-top beam. $N = 40$, SLL $= -14.2\,\mathrm{dB}$.

Table A.10: Convex method: Element positions and phase shifts, $N = 40$, SLL $= -14.2\,\mathrm{dB}$.

n	x_n (λ)	$\Delta\Phi_n$ (degrees)	n	x_n (λ)	$\Delta\Phi_n$ (degrees)
1	-9.3606	13.0857	21	0.3011	-27.2908
2	-8.6737	26.5627	22	0.8136	-1.7569
3	-8.2592	97.6007	23	1.3467	9.4626
4	-7.6851	87.1316	24	2.0902	31.2573
5	-7.2851	-179.5520	25	2.7345	37.0215
6	-6.8851	107.4687	26	3.1397	-37.9046
7	-6.4851	-158.1282	27	3.5963	-22.3647
8	-6.0851	149.5473	28	4.0381	-63.4118
9	-5.6851	-115.3319	29	4.4381	-62.4872
10	-5.0599	-97.7097	30	5.0552	-74.7847
11	-4.6599	-37.3913	31	5.4552	178.3648
12	-4.2527	-73.1332	32	5.8552	-116.9208
13	-3.8527	-9.7196	33	6.2552	137.8671
14	-3.4527	-51.2766	34	6.6552	179.2334
15	-2.9549	16.1559	35	7.0552	101.7457
16	-2.4093	32.6407	36	7.4552	147.8152
17	-1.8522	17.4919	37	7.8552	33.0857
18	-1.1901	5.3581	38	8.2552	120.6330
19	-0.6283	-21.7372	39	8.6552	28.1012
20	-0.1487	0	40	9.3606	3.6762

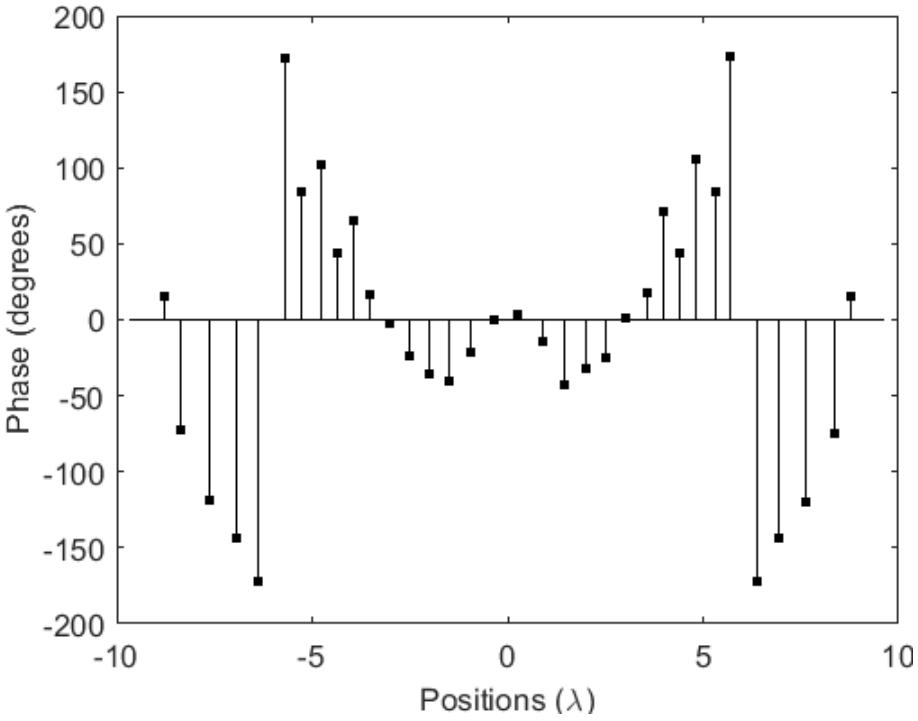

Figure A.8: Convex method: Element positions and phase shifts for the flat-top beam. $N = 34$, SLL $= -13.0\,\mathrm{dB}$.

Table A.11: Convex method: Element positions and phase shifts, $N = 34$, SLL $= -13.0\,\mathrm{dB}$.

n	x_n (λ)	$\Delta\Phi_n$ (degrees)	n	x_n (λ)	$\Delta\Phi_n$ (degrees)
1	-8.7835	15.9974	18	0.2546	3.6653
2	-8.3835	-72.7700	19	0.9030	-14.3865
3	-7.6232	-119.1037	20	1.4644	-43.3032
4	-6.9286	-143.5781	21	1.9925	-32.4389
5	-6.3774	-172.1429	22	2.5117	-25.4566
6	-5.6900	172.4077	23	3.0282	1.2134
7	-5.2900	84.5806	24	3.5711	18.0279
8	-4.7733	101.8008	25	3.9711	71.2908
9	-4.3733	44.2280	26	4.4010	43.9459
10	-3.9345	65.8308	27	4.8010	105.3364
11	-3.5345	16.0962	28	5.3095	84.6792
12	-3.0191	-1.9887	29	5.7095	173.0843
13	-2.5089	-23.4515	30	6.3930	-172.3439
14	-2.0037	-35.9177	31	6.9384	-143.3331
15	-1.4916	-40.0747	32	7.6296	-119.6819
16	-0.9585	-21.4951	33	8.3835	-74.4277
17	-0.3438	0	34	8.7835	15.4650

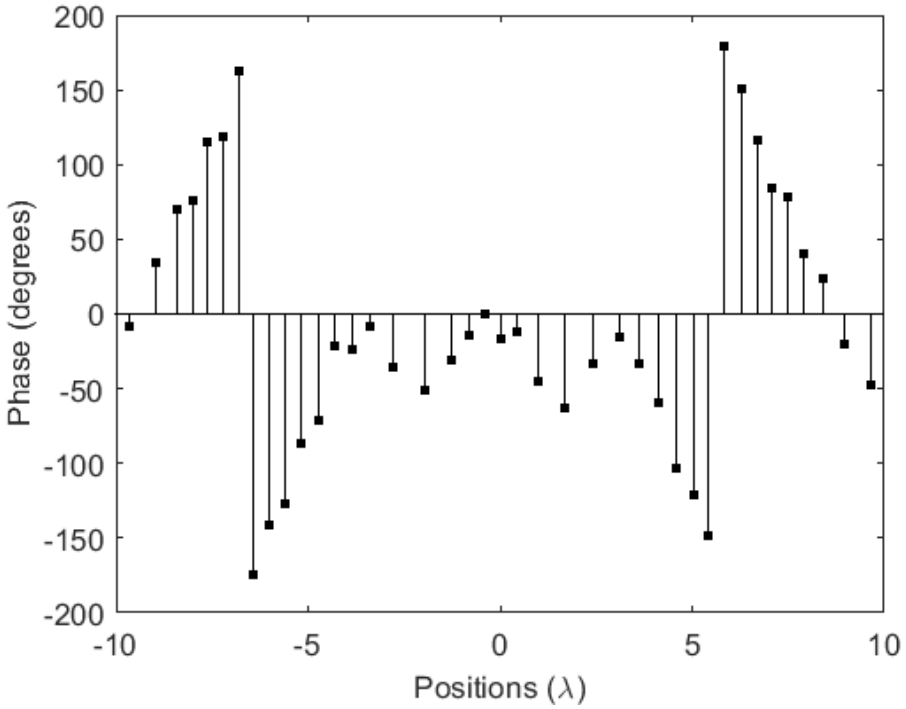

Figure A.9: Deterministic method: Element positions and phase shifts, $N = 40$, SLL $= -21.0\,\mathrm{dB}$.

Table A.12: Deterministic method: Element positions and phase shifts, $N = 40$, SLL $= -21.0$ dB.

n	x_n (λ)	$\Delta\Phi_n$ (degrees)	n	x_n (λ)	$\Delta\Phi_n$ (degrees)
1	-9.6426	-8.0210	21	0.0073	-16.8642
2	-8.9433	33.8484	22	0.4292	-11.5212
3	-8.4074	70.5309	23	0.9755	-45.5512
4	-8.0074	75.3859	24	1.6873	-63.2367
5	-7.6074	115.3961	25	2.4386	-33.1721
6	-7.2074	118.1472	26	3.0980	-15.0693
7	-6.8061	162.0308	27	3.6114	-33.6711
8	-6.4061	-174.0988	28	4.1438	-59.0203
9	-6.0061	-140.7808	29	4.5930	-103.4034
10	-5.6061	-126.8882	30	5.0275	-121.1562
11	-5.2061	-86.5524	31	5.4275	-148.5663
12	-4.7155	-71.8013	32	5.8275	179.6652
13	-4.3155	-21.9371	33	6.2963	150.7867
14	-3.8467	-24.2774	34	6.6963	116.7962
15	-3.4021	-7.7723	35	7.0963	83.9268
16	-2.7688	-36.1543	36	7.4963	77.7906
17	-1.9466	-50.6207	37	7.8963	40.8651
18	-1.2715	-31.0661	38	8.3901	24.2236
19	-0.7955	-13.6999	39	8.9417	-20.3525
20	-0.3927	0	40	9.6426	-47.6465

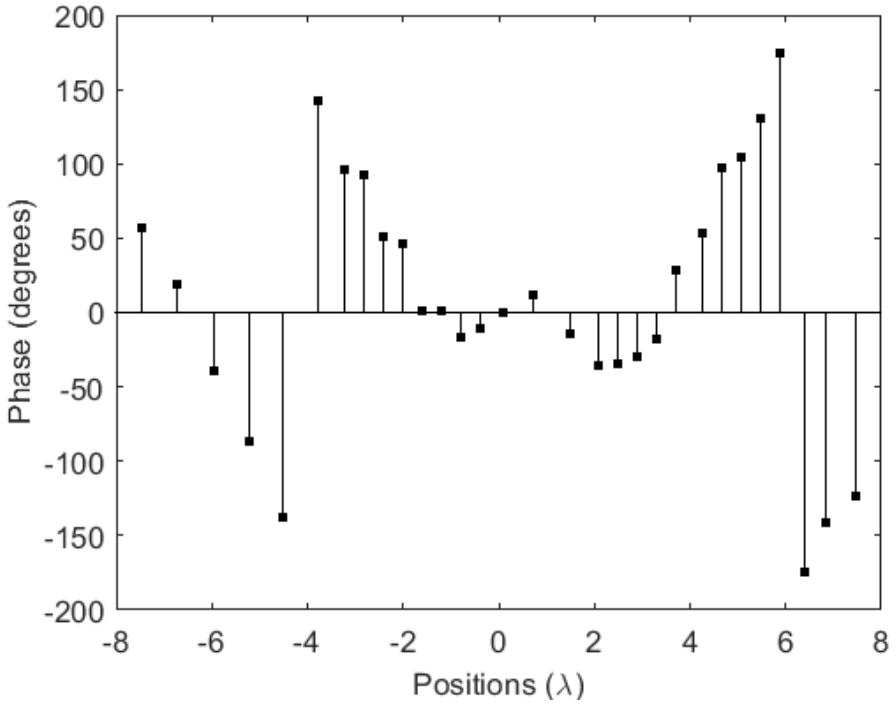

Figure A.10: Deterministic method: Element positions and phase shifts, $N = 30$, SLL $= -20.0\,\mathrm{dB}$.

Table A.13: Deterministic method: Element positions and phase shifts, $N = 30$, SLL $= -20.0\,\mathrm{dB}$.

n	x_n (λ)	$\Delta\Phi_n$ (degrees)	n	x_n (λ)	$\Delta\Phi_n$ (degrees)
1	-7.4648	57.1352	16	0.7196	11.3408
2	-6.7106	19.5786	17	1.4754	-14.6963
3	-5.9479	-39.6168	18	2.0821	-35.9016
4	-5.2318	-86.2942	19	2.4938	-34.7835
5	-4.5073	-137.5818	20	2.8975	-29.9671
6	-3.7683	142.4394	21	3.2975	-17.4439
7	-3.2276	95.8946	22	3.6982	28.3693
8	-2.8239	92.7172	23	4.2540	55.6049
9	-2.4239	51.0193	24	4.6544	97.0952
10	-2.0006	46.6066	25	5.0742	104.5003
11	-1.5966	0.8605	26	5.4742	130.3192
12	-1.1966	0.8316	27	5.8742	173.9128
13	-0.7966	-16.2604	28	6.3864	-174.5359
14	-0.3966	-10.5432	29	6.8540	-140.7509
15	-0.0843	0	30	7.4648	-123.3612

A.5 Case 5: Reconfigurable Beam

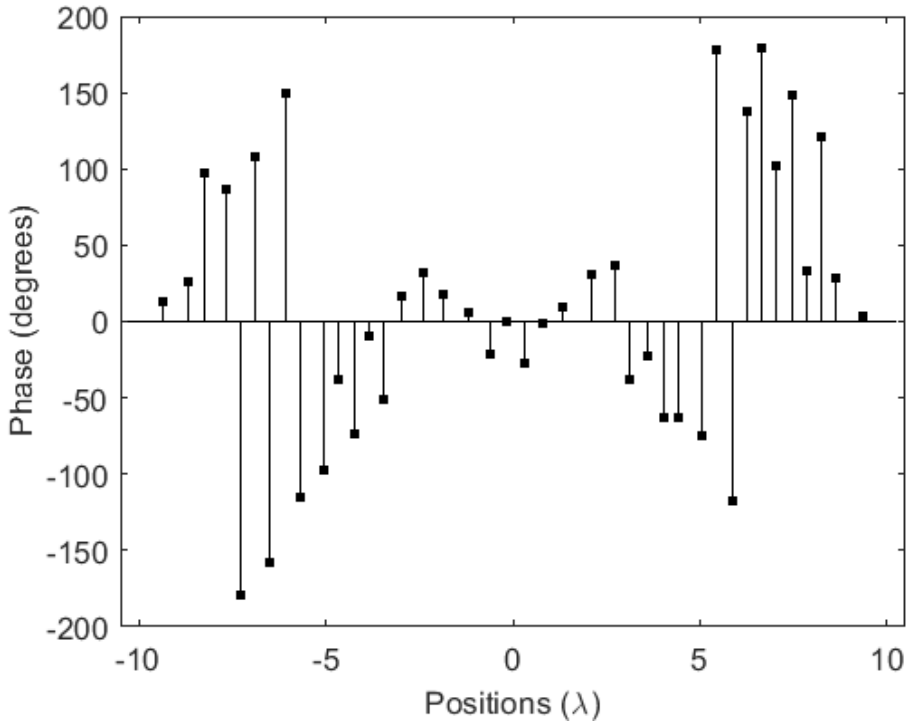

Figure A.11: Convex method: Element positions and phase shifts for the shaped beam. Reconfigurable flat-top beam, $N = 40$, SLL $= -14.2\,\mathrm{dB}$.

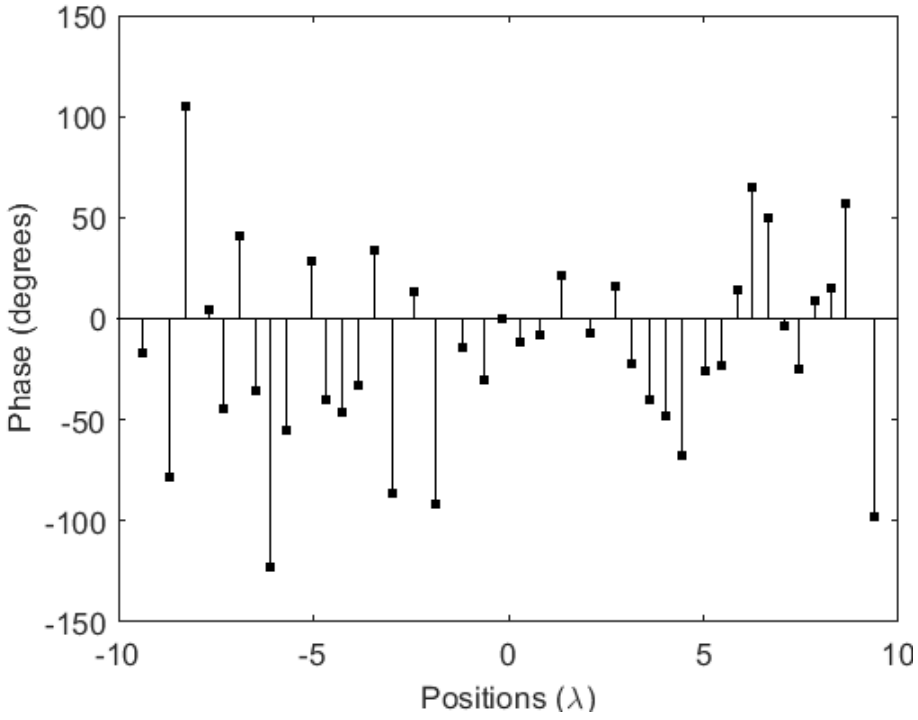

Figure A.12: Convex method: Element positions and phase shifts for the pencil beam. Reconfigurable flat-top beam, $N = 40$, SLL $= -13.2\,\mathrm{dB}$.

Table A.14: Convex method: Element positions and phase shifts for flat-top reconfigurable beams, $N = 40$, SLL $= -14.2\,\text{dB}$, pencil SLL $= = -13.2\,\text{dB}$.

n	x_n (λ)	$\Delta\Phi_n$ (degrees) Shaped beam	$\Delta\Phi_n$ (degrees) Pencil beam
1	-9.3606	13.0857	-17.1108
2	-8.6737	26.5627	-78.3720
3	-8.2592	97.6007	105.3892
4	-7.6851	87.1316	4.7656
5	-7.2851	-179.5520	-44.8901
6	-6.8851	107.4687	41.2823
7	-6.4851	-158.1282	-35.7035
8	-6.0851	149.5473	-123.1610
9	-5.6851	-115.3319	-54.9538
10	-5.0599	-97.7097	28.8760
11	-4.6599	-37.3913	-39.9706
12	-4.2527	-73.1332	-45.8746
13	-3.8527	-9.7196	-32.8776
14	-3.4527	-51.2766	33.9791
15	-2.9549	16.1559	-86.3635
16	-2.4093	32.6407	12.9083
17	-1.8522	17.4919	-91.9087
18	-1.1901	5.3581	-14.6265
19	-0.6283	-21.7372	-30.6846
20	-0.1487	0	0
21	0.3011	-27.2908	-11.8850
22	0.8136	-1.7569	-7.7718
23	1.3467	9.4626	21.1360
24	2.0902	31.2573	-7.3647
25	2.7345	37.0215	16.0390
26	3.1397	-37.9046	-22.1397
27	3.5963	-22.3647	-40.4199
28	4.0381	-63.4118	-48.2886
29	4.4381	-62.4872	-67.8640
30	5.0552	-74.7847	-25.4429
31	5.4552	178.3648	-23.4733
32	5.8552	-116.9208	12.1065
33	6.2552	137.8671	65.0338
34	6.6552	179.2334	49.7638
35	7.0552	101.7457	-3.2419
36	7.4552	147.8152	-24.6483
37	7.8552	33.0857	8.6201
38	8.2552	120.6330	15.5283
39	8.6552	28.1012	56.7164
40	9.3606	3.6762	-98.3505

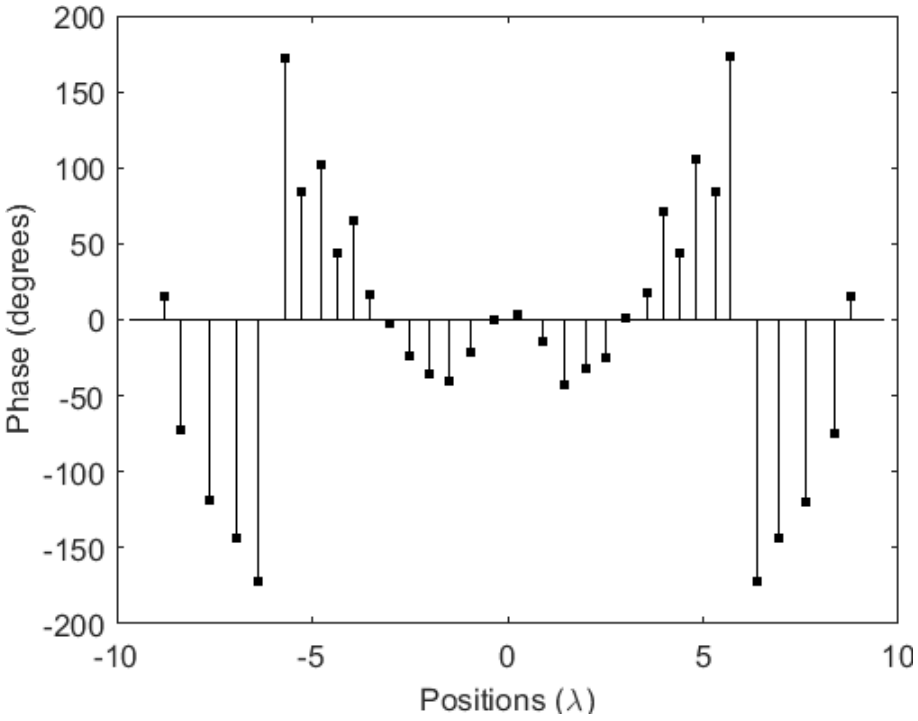

Figure A.13: Convex method: Element positions and phase shifts for the shaped beam. Reconfigurable flat-top beam, $N = 34$, SLL $= -13.0\,\mathrm{dB}$.

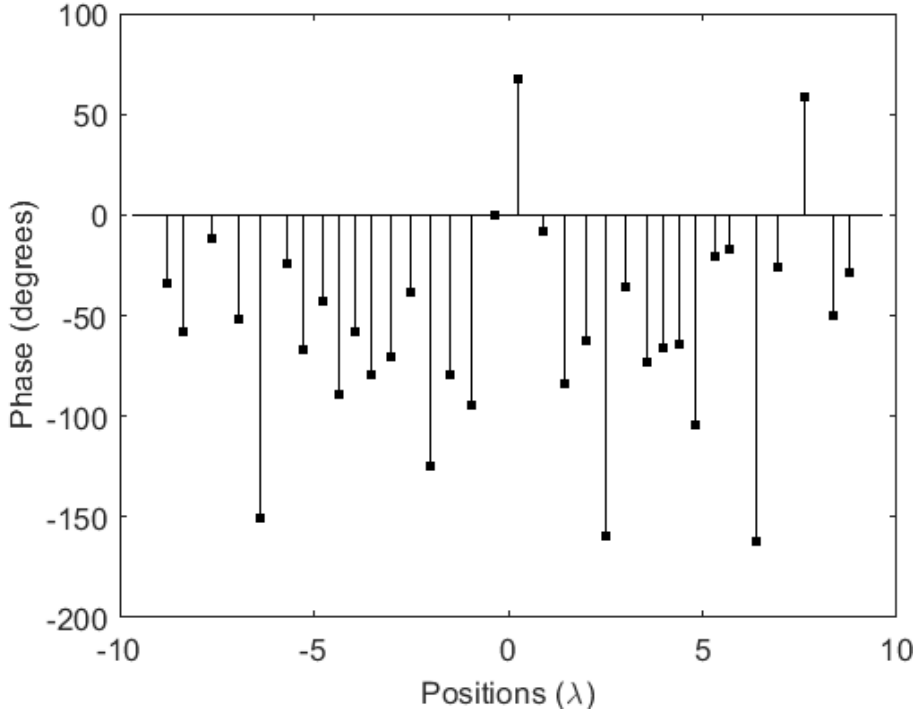

Figure A.14: Convex method: Element positions and phase shifts for the pencil beam. Reconfigurable flat-top beam, $N = 34$, SLL $= -11.3\,\mathrm{dB}$.

Table A.15: Convex method: Element positions and phase shifts for flat-top reconfigurable beams, $N = 34$, SLL $= -13.0\,\text{dB}$, pencil SLL $= = -11.3\,\text{dB}$.

n	x_n (λ)	$\Delta\Phi_n$ (degrees) Shaped beam	$\Delta\Phi_n$ (degrees) Pencil beam
1	-8.7835	15.9974	-34.1758
2	-8.3835	-72.7700	-58.2105
3	-7.6232	-119.1037	-11.9708
4	-6.9286	-143.5781	-51.5962
5	-6.3774	-172.1429	-150.7504
6	-5.6900	172.4077	-24.3550
7	-5.2900	84.5806	-67.2981
8	-4.7733	101.8008	-42.5516
9	-4.3733	44.2280	-89.1488
10	-3.9345	65.8308	-58.2207
11	-3.5345	16.0962	-79.2979
12	-3.0191	-1.9887	-70.4380
13	-2.5089	-23.4515	-38.8366
14	-2.0037	-35.9177	-124.5769
15	-1.4916	-40.0747	-79.3804
16	-0.9585	-21.4951	-94.3173
17	-0.3438	0	0
18	0.2546	3.6653	67.1057
19	0.9030	-14.3865	-8.5628
20	1.4644	-43.3032	-84.2462
21	1.9925	-32.4389	-62.3386
22	2.5117	-25.4566	-159.0582
23	3.0282	1.2134	-36.0782
24	3.5711	18.0279	-72.8269
25	3.9711	71.2908	-66.3031
26	4.4010	43.9459	-63.8936
27	4.8010	105.3364	-104.3684
28	5.3095	84.6792	-20.9743
29	5.7095	173.0843	-17.1985
30	6.3930	-172.3439	-162.2802
31	6.9384	-143.3331	-25.7654
32	7.6296	-119.6819	58.7840
33	8.3835	-74.4277	-50.1957
34	8.7835	15.4650	-28.6040

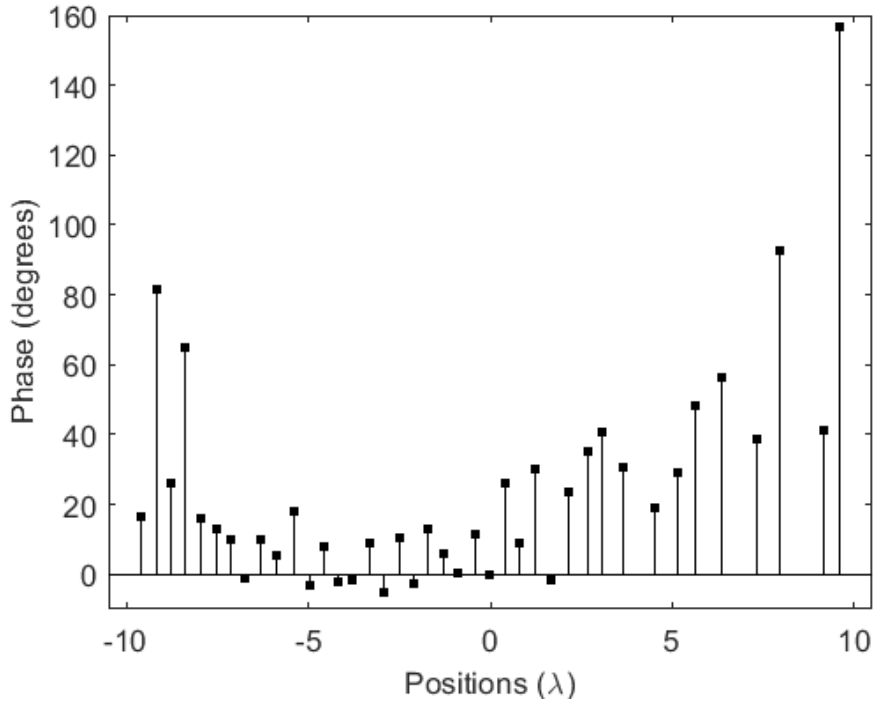

Figure A.15: Deterministic method: Element positions and phase shifts for the shaped beam. Reconfigurable cosecant squared beam, $N = 40$, SLL $= -19.0\,\mathrm{dB}$.

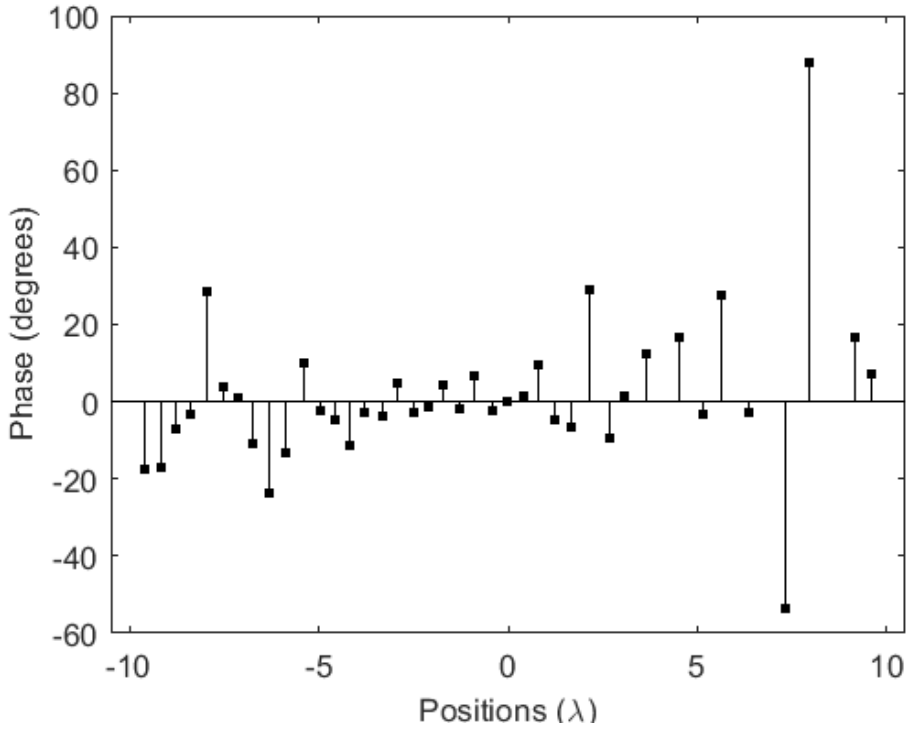

Figure A.16: Deterministic method: Element positions and phase shifts for the pencil beam. Reconfigurable cosecant squared beam, $N = 40$, SLL $= -19.0\,\mathrm{dB}$.

Table A.16: Deterministic method: Element positions and phase shifts for cosecant squared reconfigurable beams, $N = 40$, SLL $= -19.0\,\mathrm{dB}$.

n	x_n (λ)	$\Delta\Phi_n$ (degrees) Shaped beam	$\Delta\Phi_n$ (degrees) Pencil beam
1	-9.5829	16.6471	-17.7120
2	-9.1829	81.7032	-16.8989
3	-8.7829	25.8804	-7.0565
4	-8.3829	64.8535	-3.0659
5	-7.9829	15.9171	28.5057
6	-7.5356	13.0028	3.8806
7	-7.1356	9.7708	1.0100
8	-6.7356	-0.9318	-10.7294
9	-6.2910	9.7388	-23.8698
10	-5.8570	5.3586	-13.0734
11	-5.3838	17.7454	10.1715
12	-4.9838	-3.0337	-2.2746
13	-4.5838	8.1003	-4.5733
14	-4.1838	-2.3068	-11.1794
15	-3.7757	-1.5488	-2.5912
16	-3.3260	9.0605	-3.8449
17	-2.9165	-5.1741	4.8163
18	-2.4964	10.3403	-2.8701
19	-2.0964	-2.6812	-1.2012
20	-1.6964	13.0868	4.4891
21	-1.2964	5.9535	-1.7998
22	-0.8964	0.1968	6.6189
23	-0.4145	11.6223	-2.1135
24	-0.0145	0	0
25	0.4130	26.2727	1.4849
26	0.8130	8.6934	9.4448
27	1.2555	30.3251	-4.5585
28	1.6555	-1.4801	-6.4036
29	2.1583	23.5692	28.9916
30	2.6691	35.2321	-9.4543
31	3.0691	40.5469	1.5414
32	3.6508	30.5913	12.3171
33	4.5159	19.0169	16.5910
34	5.1539	29.0145	-3.4318
35	5.6247	48.4546	27.6939
36	6.3481	56.2814	-2.7941
37	7.3434	38.5282	-53.4025
38	7.9541	92.8386	87.8884
39	9.1829	40.9894	16.5529
40	9.5829	156.8214	7.3278

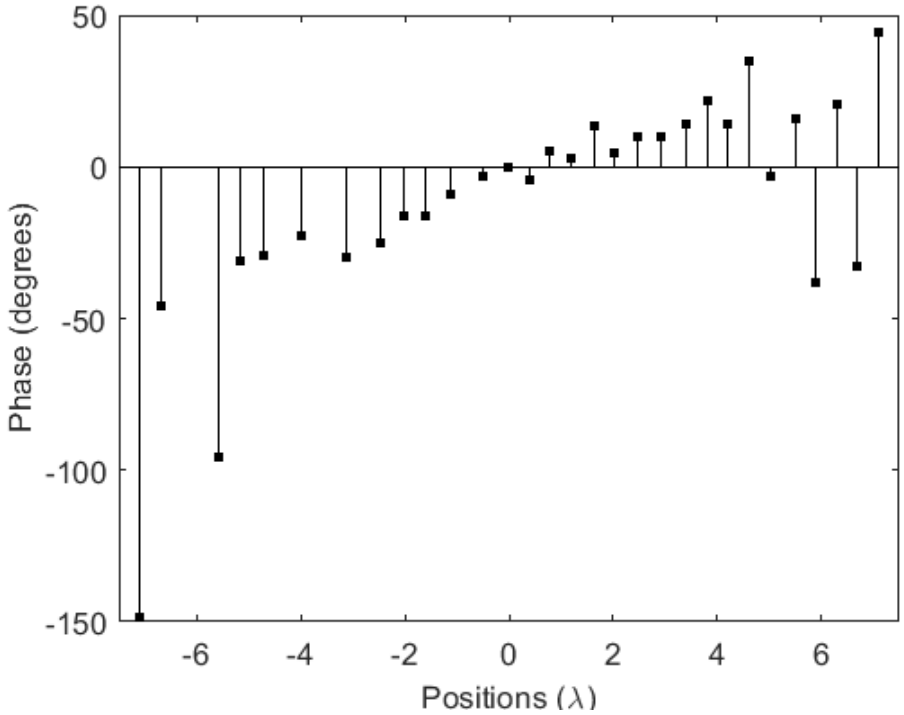

Figure A.17: Deterministic method: Element positions and phase shifts for the shaped beam. Reconfigurable cosecant squared beam, $N = 30$, SLL $= -16.0\,\mathrm{dB}$.

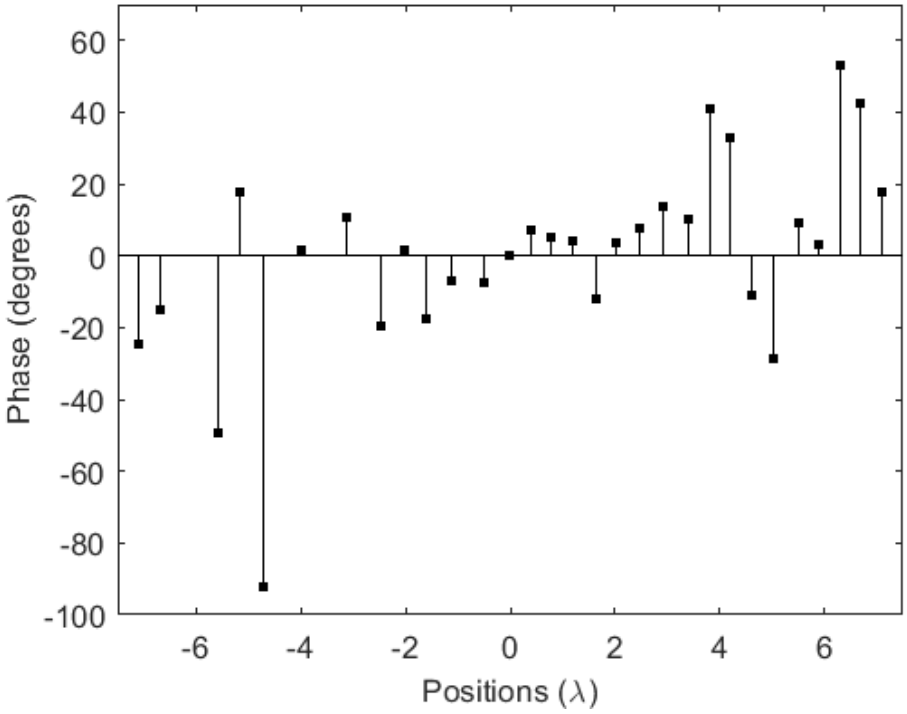

Figure A.18: Deterministic method: Element positions and phase shifts for the pencil beam. Reconfigurable cosecant squared beam, $N = 30$, SLL $= -16.0\,\mathrm{dB}$.

Table A.17: Deterministic method: Element positions and phase shifts for cosecant squared reconfigurable beams, $N = 30$, SLL $= -16.0\,\mathrm{dB}$.

n	x_n (λ)	$\Delta\Phi_n$ (degrees) Shaped beam	$\Delta\Phi_n$ (degrees) Pencil beam
1	-7.1024	-148.3023	-24.8147
2	-6.7024	-45.7866	-15.2428
3	-5.5937	-95.6877	-49.3200
4	-5.1640	-31.0401	17.9851
5	-4.7078	-29.2918	-92.2799
6	-4.0000	-22.9488	1.6891
7	-3.1427	-30.0463	10.8394
8	-2.4559	-25.1555	-19.6270
9	-2.0110	-16.0947	1.6278
10	-1.6110	-16.3980	-17.4388
11	-1.1361	-9.1300	-7.0901
12	-0.5138	-2.9274	-7.5448
13	-0.0167	0	0
14	0.3833	-4.4485	6.9992
15	0.7946	5.0526	5.2159
16	1.1946	2.9975	4.1000
17	1.6315	13.2369	-12.2123
18	2.0315	4.5869	3.5024
19	2.4872	9.6618	7.5861
20	2.9309	10.2343	13.5155
21	3.4087	14.2070	10.3457
22	3.8122	21.6880	41.1180
23	4.2122	14.2666	33.1615
24	4.6158	34.7620	-10.9526
25	5.0158	-3.3792	-28.8115
26	5.5024	16.0241	9.1458
27	5.9024	-38.1355	3.3240
28	6.3024	20.7750	53.2703
29	6.7024	-32.5860	42.2660
30	7.1024	44.6544	17.5656

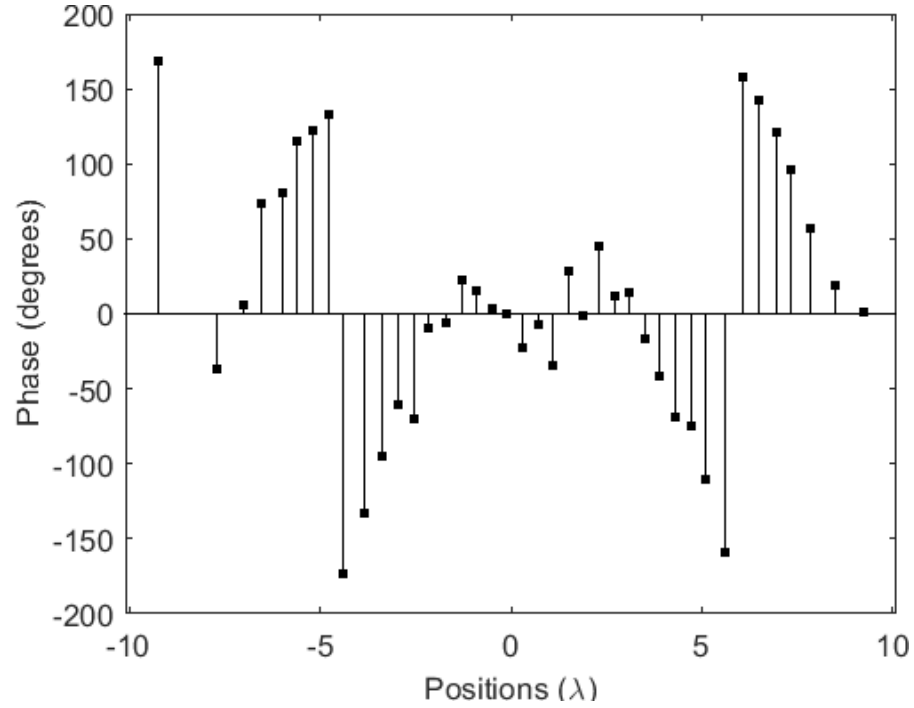

Figure A.19: Deterministic method: Element positions and phase shifts for the shaped beam. Reconfigurable flat-top beam, $N = 40$, SLL $= -18.0\,\mathrm{dB}$.

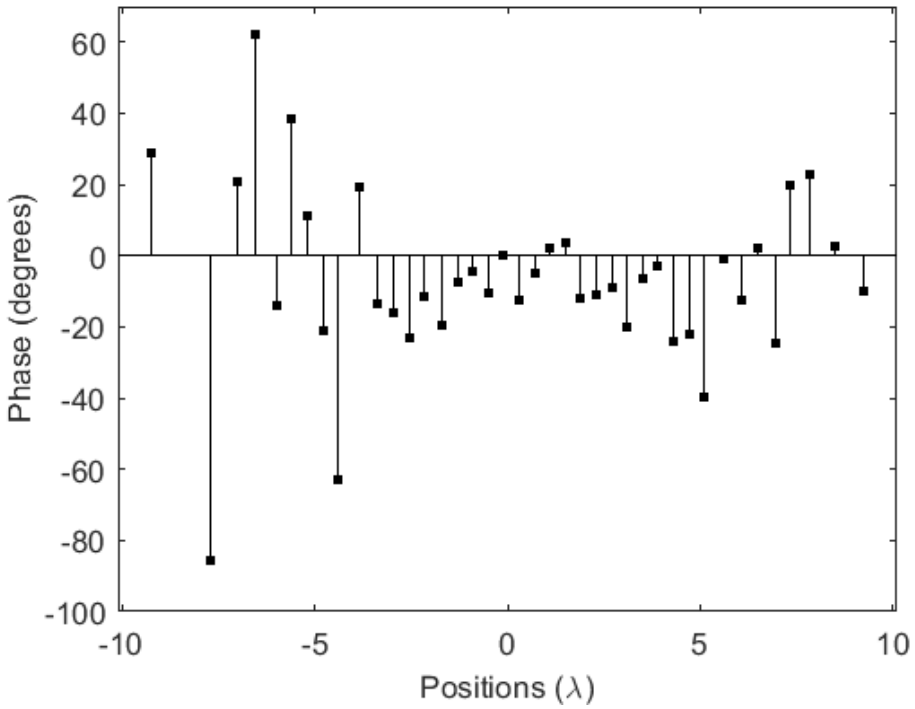

Figure A.20: Deterministic method: Element positions and phase shifts for the pencil beam. Reconfigurable flat-top beam, $N = 40$, SLL $= -18.0\,\mathrm{dB}$.

Table A.18: Deterministic method: Element positions and phase shifts for flat-top reconfigurable beams, $N = 40$, SLL $= -18.0$ dB.

n	x_n (λ)	$\Delta\Phi_n$ (degrees) Shaped beam	$\Delta\Phi_n$ (degrees) Pencil beam
1	-9.2210	168.8947	28.7391
2	-7.7066	-36.6077	-85.4645
3	-7.0032	6.4596	20.8453
4	-6.5380	73.0433	62.4304
5	-5.9882	80.4035	-14.0909
6	-5.5882	115.1720	38.6710
7	-5.1882	121.7925	11.0890
8	-4.7882	132.9472	-20.8497
9	-4.3882	-173.0498	-63.0059
10	-3.8252	-132.8569	19.2954
11	-3.3844	-95.4723	-13.3337
12	-2.9715	-60.6903	-15.8926
13	-2.5587	-69.5074	-22.8451
14	-2.1587	-9.4395	-11.6393
15	-1.6932	-5.3617	-19.7245
16	-1.2932	23.1037	-7.2482
17	-0.8932	15.1103	-4.2590
18	-0.4932	3.8380	-10.3388
19	-0.0932	0	0
20	0.3068	-22.9269	-12.3335
21	0.7068	-7.5018	-4.7808
22	1.1068	-34.7676	2.2071
23	1.5068	28.6846	3.4132
24	1.9068	-0.9798	-12.2066
25	2.3068	45.4128	-11.0575
26	2.7068	12.3569	-8.7604
27	3.1068	14.6130	-19.8333
28	3.5068	-16.4527	-6.4273
29	3.9068	-41.2920	-3.1046
30	4.3068	-68.2881	-24.1473
31	4.7068	-74.6509	-22.2077
32	5.1068	-110.3638	-39.7748
33	5.6238	-158.6811	-1.0779
34	6.0880	157.9370	-12.2764
35	6.4880	141.9780	2.2210
36	6.9374	120.9495	-24.7206
37	7.3374	95.9293	19.5784
38	7.8467	57.4388	22.8430
39	8.5057	18.8680	2.5377
40	9.2210	1.5256	-9.9228

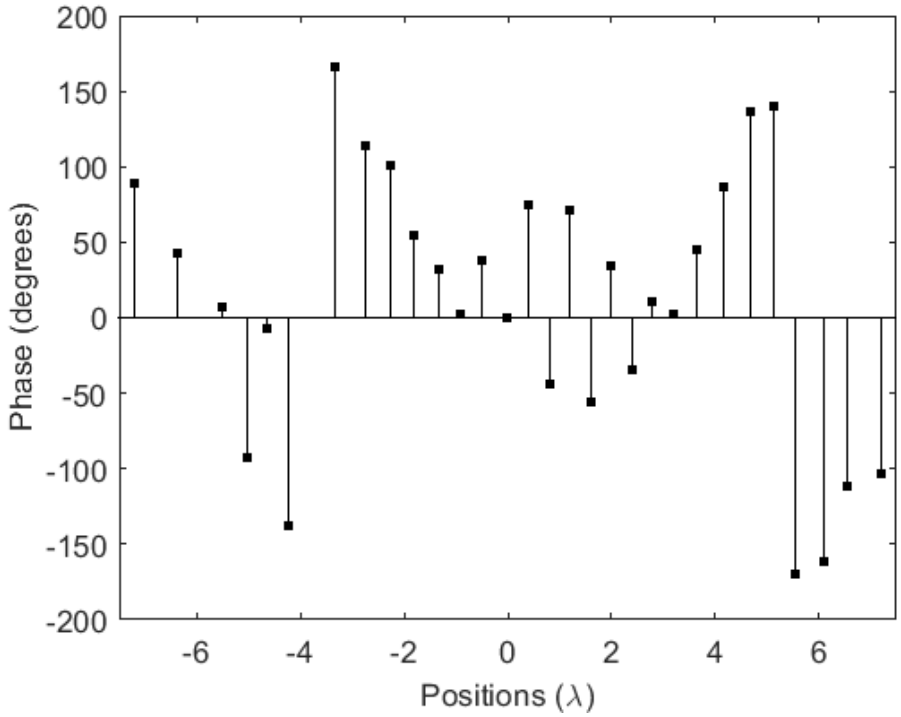

Figure A.21: Deterministic method: Element positions and phase shifts for the shaped beam. Reconfigurable flat-top beam, $N = 30$, SLL $= -16.0\,\mathrm{dB}$.

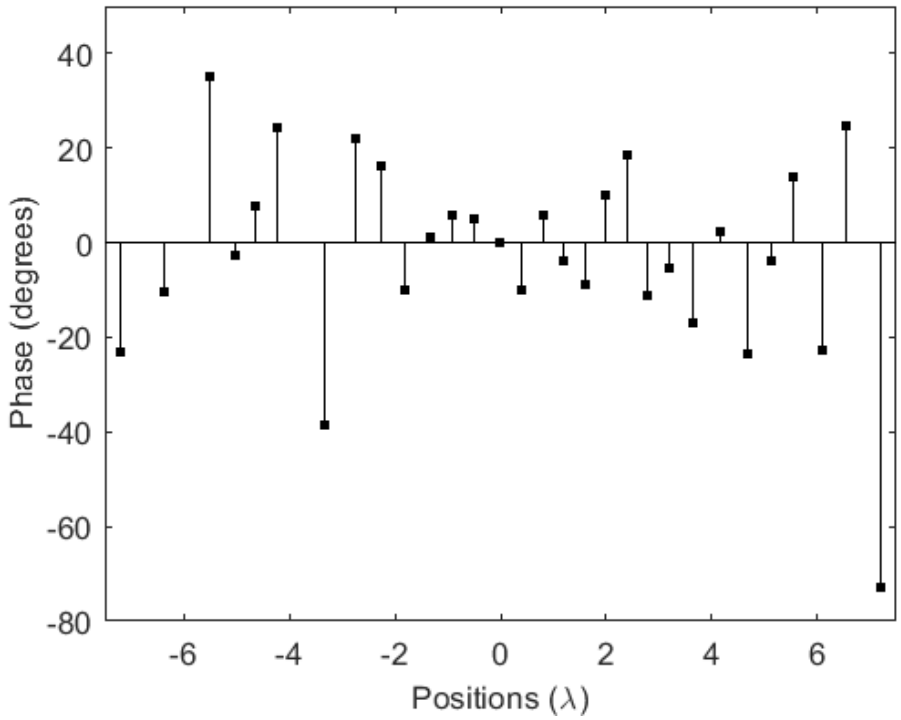

Figure A.22: Deterministic method: Element positions and phase shifts for the pencil beam. Reconfigurable flat-top beam, $N = 30$, SLL $= -16.0\,\mathrm{dB}$.

Table A.19: Deterministic method: Element positions and phases for flat-top reconfigurable beams, $N = 30$, SLL $= -16.0$ dB.

n	x_n (λ)	$\Delta\Phi_n$ (degrees) Shaped beam	$\Delta\Phi_n$ (degrees) Pencil beam
1	-7.1962	89.0923	-23.2693
2	-6.3703	42.6342	-10.4757
3	-5-5152	7.4140	35.3258
4	-5.0458	-92.8281	-2.4841
5	-4.6458	-7.4932	7.9155
6	-4.2458	-138.0428	24.5117
7	-3.3462	165.7520	-38.5517
8	-2.7558	113.5571	22.1120
9	-2.2800	100.9151	16.1259
10	-1.8078	54.8572	-10.1410
11	-1.3145	31.7237	1.3803
12	-0.9145	1.8720	5.8604
13	-0.4920	37.7817	4.9156
14	-0.0041	0	0
15	0.3959	74.8063	-9.7970
16	0.7959	-43.4342	5.7398
17	1.1959	71.5972	-3.9446
18	1.5959	-55.6967	-9.0118
19	1.9959	34.8708	9.9488
20	2.3959	-34.4346	18.4991
21	2.7959	10.3803	-11.3056
22	3.1959	2.2709	-5.2237
23	3.6571	45.6168	-16.7841
24	4.1817	86.0935	2.3249
25	4.6666	136.9257	-23.5977
26	5.1434	139.7370	-3.8017
27	5.5434	-170.0811	13.8264
28	6.0894	-161.6577	-22.8118
29	6.5481	-111.6645	24.8017
30	7.1962	-102.8124	-72.7309

DEPARTMENT OF SOME SUBJECT OR TECHNOLOGY
CHALMERS UNIVERSITY OF TECHNOLOGY
Gothenburg, Sweden
www.chalmers.se

CHALMERS
UNIVERSITY OF TECHNOLOGY